https://ntrs.nasa.gov/search.jsp?R=19820003579 2020-03-21T11:30:32+00:00Z

NASA
CR
3477
c.1

TECH LIBRARY KAFB, NM
0062243

NASA Contractor Report 3477

InGaAsP/InP Laser Development for Single-Mode, High-Data-Rate Communications

LOAN COPY: RETURN TO
AFWL TECHNICAL LIBRARY
KIRTLAND AFB, N.M.

I. Ladany, E. R. Levin, C. W. Magee,
and R. T. Smith

CONTRACT NAS1-15962
NOVEMBER 1981

NASA

TECH LIBRARY KAFB, NM

0062243

NASA Contractor Report 3477

InGaAsP/InP Laser Development for Single-Mode, High-Data-Rate Communications

I. Ladany, E. R. Levin, C. W. Magee,
and R. T. Smith
RCA Laboratories
Princeton, New Jersey

Prepared for
Langley Research Center
under Contract NAS1-15962

National Aeronautics
and Space Administration

Scientific and Technical
Information Branch

1981

PREFACE

This Interim Report covers work performed at RCA Laboratories during the period July 1, 1980 to March 31, 1981 under Contract No. NAS1-15962. The Laboratory Director was B. Hershenov, the Group Head was M. E. Ettenberg, and the Project Scientist was I. Ladany. The COTR was H. Hendricks, NASA Langley Research Center, Hampton, Virginia.

Staff members and support personnel who contributed to this work in addition to the authors, and the area of their contributions, are listed below.

E. P. Bertin*	-	EPMA
N. DiGiuseppe	-	Photoluminescence
T. Furman	-	LPE growth
D. Gilbert	-	Device measurements
F. Z. Hawrylo*	-	LPE growth
M. Harvey	-	Device fabrication
H. Kowger	-	Device fabrication
D. P. Marinelli	-	Device fabrication
S. H. McFarlane, III*	-	X-ray topography
G. H. Olsen*	-	Photodetectors

*Member Technical Staff.

TABLE OF CONTENTS

Section		Page
INTRODUCTION		1
I.	MATERIALS STUDIES	2
	A. Dislocation Measurement	2
	B. Pullover	6
II.	GENERAL DEVICE STUDIES	20
	A. Acceptor Doping	20
	B. EBIC Measurements	23
	C. Ohmic Contact to P-Side	26
	D. Minimum Threshold Current Density	28
III.	SINGLE-MODE LASER DEVELOPMENT	31
	A. General Approach to Single-Mode Laser Fabrication.	31
	B. Device Results: CDH and MSBH	40
	C. Device Results: Buried Heterojunction (BH)	42
IV.	LONG-WAVELENGTH PHOTODETECTORS	47
V.	CONCLUSIONS	48
	REFERENCES	50

LIST OF ILLUSTRATIONS

Figure		Page
1.	Comparison of x-ray topograph (a) and CL image (b) of same wafer (but not necessarily same area). The large spot in (b) is an artifact caused by damage induced during CL scan	3
2.	Typical InP wafer used in this work as it appears after etching in Huber etch. A portion of this figure is shown further magnified in Fig. 3	5
3.	Individual etch pits are easily resolved and correspond to areas where dislocations make steep angles with the surface	6
4.	X-ray topograph (400/Mo) of typical InP wafer used in this work	7
5.	Schematic indicating layer thicknesses and the composition of the active and cap quaternary layers	9
6.	X-ray diffraction patterns of the (a) anomalous and (b) normal wafer. The quaternary cap layer was removed by etching before these patterns were taken	10
7.	Room-temperature photoluminescence scans using argon ion laser excitation. Trace I is obtained from the anomalous wafer after the quaternary cap layer is removed. Trace II results when the p-type cladding layer is also removed	12
8.	SIMS profiles through the anomalous wafer	13
9.	SIMS profiles through the normal wafer	14
10.	Experimental values for the distribution coefficients. Solid lines shown extrapolated values of reference 3	17

LIST OF ILLUSTRATIONS (Continued)

Figure		Page
11.	Angle lap photomicrographs through the normal (a and c) and the anomalous (b and d) wafers	19
12.	In/Zn alloy used for acceptor doping. Upper part of the figure shows the slice of material used in the analysis, and the lower part of the figure shows the points where EDXRA counts were made and the corresponding count ratios for Zn/In. A uniform composition would yield a constant ratio. Result of atomic absorption analysis for the two pieces of material separated along the dotted line shown at the bottom	21
13.	(a) Dot map showing distribution of Zn and corresponding SEM image of section of nominal In-2% Zn alloy. (b) Higher magnification SEM of same specimen. It can be seen that globules (marked B, F, G) give higher Zn/In x-ray intensity ratios and intermediate areas give low ratios	22
14.	EBIC scans of two Zn-doped samples (#480) and of one Cd-doped sample (#510). The location of the junction, taken to be at the peak of the EBIC signal, is seen to be in different regions of the structure	24
15.	SIMS profiles through the ohmic contact to the p side of a typical device. As and Au profiles for no sintering and for two different sintering temperatures are shown. Gold was removed from the surface of unsintered and 320°C sintered samples prior to analysis	27

LIST OF ILLUSTRATIONS (Continued)

Figure		Page
16.	Threshold current density versus length for low threshold material	29
17.	Examples of one-step and two-step growth of index-guided material	32
18.	The four possible groove configurations for growth on the (100) plane. (a) Inverted V groove, (b) V groove, (c) inverted raised V mesa, and (d) raised V mesa	34
19.	Growth on inverted V grooves. (a) Etched substrate, (b) schematic of etched pattern, (c) grown regions shown in optical photomicrograph, and (d) schematic of growth in (c)	35
20.	Growth in V groove, showing (a) grown layer, (b) schematic of substrate, and (c) schematic of grown layers	36
21.	Growth on raised V mesa, showing (a) substrate cross section, (b) substrate schematic, (c) completed growth, and (d) schematic of grown layers	38
22.	Growth on raised inverted V mesa. The top part of the figure shows the schematic drawing of the grown layers, and the bottom part of the figure shows an etched cross section through a grown structure	39
23.	Optical photomicrographs through MSBH type structures grown on inverted V mesas. (a) Shows the substrate after etching, (b) the completed growth, and (c) an angle lap through the grown structure	41

LIST OF ILLUSTRATIONS (Continued)

Figure		Page
24.	Different mesas etched into grown layers for BH fabrication. (a) and (b) using bromine-methanol, and (c) iodic acid etch	43
25.	Optical photomicrograph through a BH laser. The well-isolated cavity is clearly visible	43
26.	BH cavity as shown by SEM	44
27.	Near field scan through a lasing BH diode, (a) at 3 mW showing a single spot, and (b) at 5 mW where the output breaks up into two modes	44
28.	Spectrum of diode of Fig. 27, at two different currents	45
29.	Power-current relation for the laser of Fig. 27 ..	46

INTRODUCTION

In a previous program sponsored by NASA-Langley Research Center [1], RCA developed a basic growth technology for the fabrication of 1.3-μm cw laser diodes. The present study concentrated on the further advancement of this liquid-phase epitaxy (LPE) technology toward the development of index-guided single-mode 1.3-μm lasers. In addition to materials and growth related work, this study includes a systematic investigation of a number of single-mode structures. This work led to the achievement of planar devices with threshold current densities of 1000 A/cm^2 and a single-mode buried heterojunction device with a cw threshold current of 60 mA.

It is by now well known that InGaAsP lasers have assumed such a great importance in the area of communications because they allow the transmission of signals over enormous ranges (perhaps 100 km) without the need for repeaters. Not only are such systems relatively insensitive to external interference, but they also rely on glass fibers rather than copper as the conduit, and thus offer advantages in radiation resistance, cost, weight, size, and use of strategic materials. The interest of NASA in this area arises because of weight reductions possible in aircraft control systems, the high radiation-tolerance needed in intrasatellite communications, and because of many other specific applications.

I. MATERIALS STUDIES

A. DISLOCATION MEASUREMENT

One of the persistent questions that arises in the course of device development work is what effect dislocations have on device properties. Certain properties of dislocations have been known for many years. For example, it has been argued that they attract impurities or defects, and thereby improve the radiative efficiency in other regions of a wafer. Further, it is possible that they cause a direct low-impedance path across a pn junction thereby shorting the device, and it has also been thought that they may affect growth properties. It is certainly true that a great deal of work remains to be done in this area, especially when one realizes that various III-V compound crystals may behave quite differently in this respect. It might be pointed out that one of the factors giving impetus to this area of investigation is the extremely variable yield obtained in lasers fabricated from the same wafer. Thus, sometimes as many as 80% of the chips produce acceptable cw lasers, and at other times the percentage is lower by a factor of 4 or 5. A persistent question, to which so far no clear answers have been given, is what effect dislocations may have on these statistics.

1. Methods for Revealing Dislocations

We have examined the dislocation structure of InP substrates using three methods: X-ray topography, chemical etching, and cathodoluminescence (CL) mode SEM.

X-ray topography is of course well known, and may be considered the "classical" method used to calibrate the other two. An example is seen in Fig. 1(a) where an InP crystal polished in the (100) plane and containing a grain boundary line is displayed. The difference between the two regions is obvious, and the reasons for this would be highly

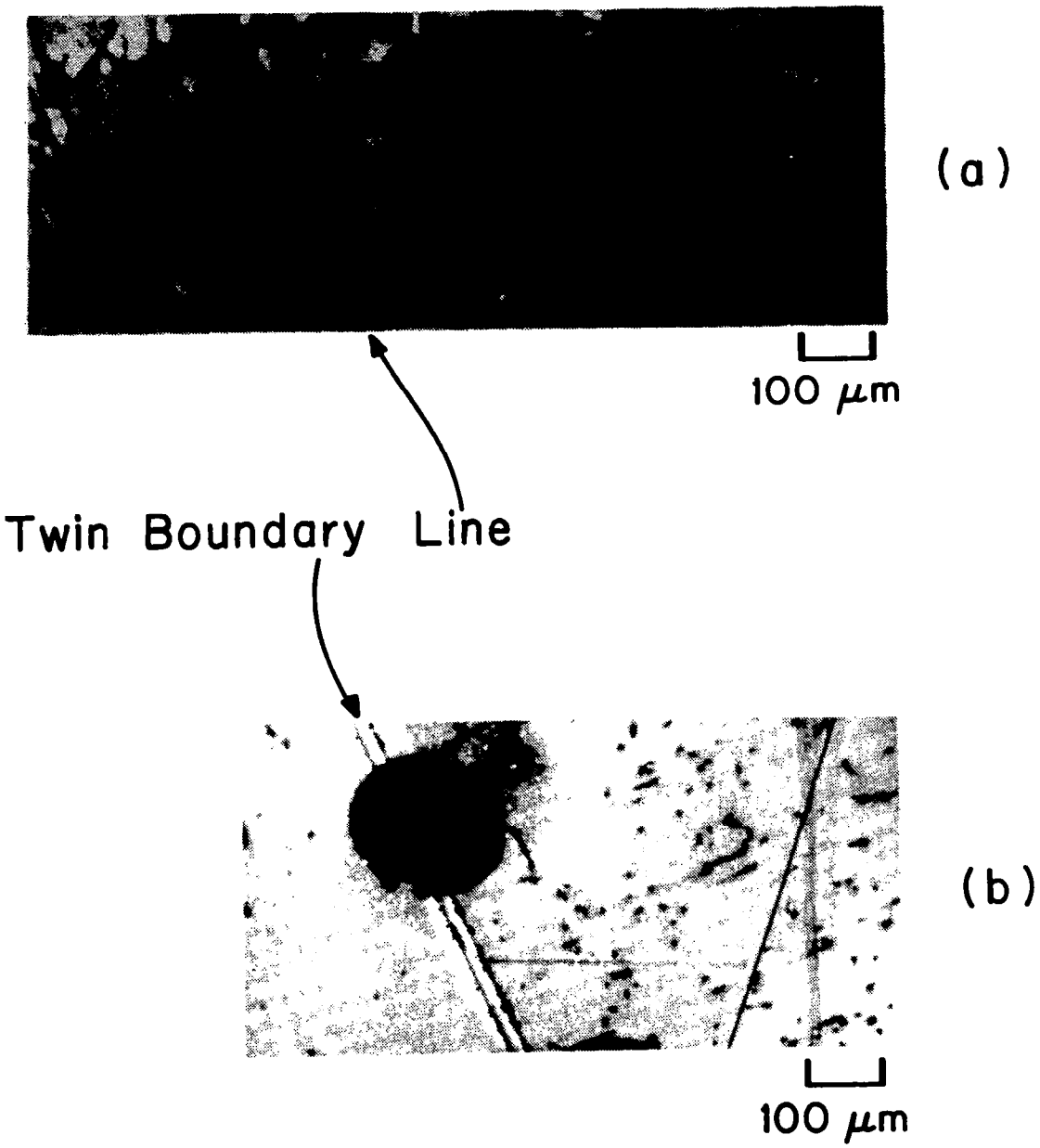

Figure 1. Comparison of x-ray topograph (a) and CL image (b) of same wafer (but not necessarily same area). The large spot in (b) is an artifact caused by damage induced during CL scan.

significant to those growing bulk crystals (this material was kindly supplied by G. Antypas).

The dislocation density on the two sides of the twin boundary differs by at least a factor of 5, being $\sim 5 \times 10^3$ cm^{-2} on the low side and $\sim 2.5 \times 10^4$ cm^{-2} on the high side. The topograph reveals dislocations positioned at various angles whereas CL only shows dark spots and short line segments where inclined dislocations intersect the surface. Using the usual counting procedures, similar values are obtained from both methods. The dark spot seen in Fig. 1 is caused by crystal damage produced during CL observation in the SEM and should be ignored.

The result of the chemical etch method is shown in Fig. 2, applied to a wafer typical of those used as substrates in the course of this work. Use of the Huber* [2] etch reveals a very complex and irregular structure showing a number of microscopic features which may be grown in or related to polishing or other process steps. The small square indicated in Fig. 2 is enlarged in Fig. 3 so that an etch pit count can be made with little difficulty. It has been established that this etch reveals steep angle dislocations crossing the surface so that the results are entirely equivalent to those obtained by CL.

Material similar to that used for Fig. 3 has been used to obtain the topograph shown in Fig. 4, where a number of features are visible in addition to dislocations. There is little doubt that our standard substrate material contains numerous faults which are bound to manifest themselves in device properties.

In terms of convenience, chemical etching is clearly the preferred method for revealing the presence of dislocations. Thus, as better substrate material becomes available, it should be possible to study the connection between crystal faults and device properties.

*2 vol [85% H_3PO_4]: 1 vol [HBr 47%] at 24°C for 2 minutes.

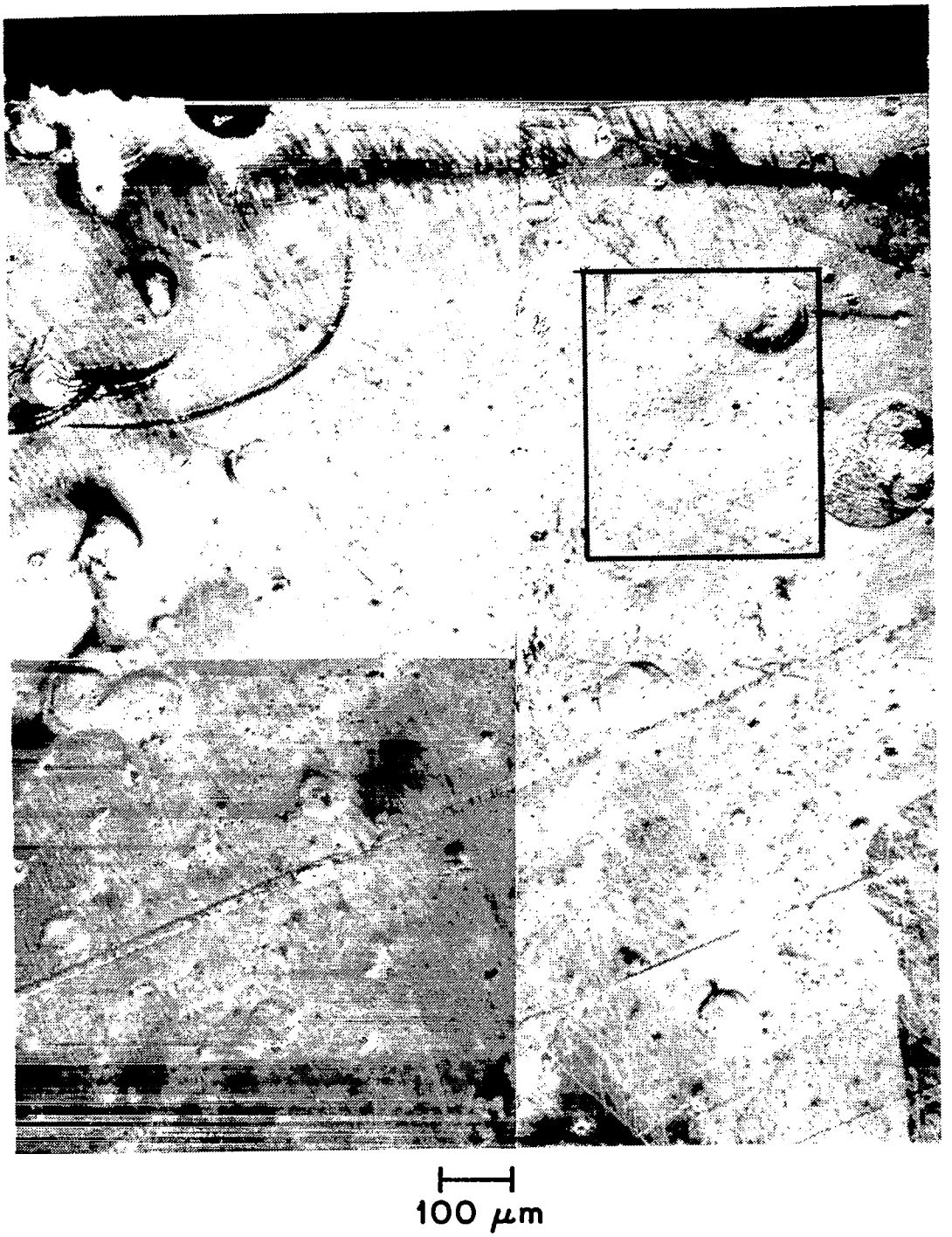

Figure 2. Typical InP wafer used in this work as it appears after etching in Huber etch. A portion of this figure is shown further magnified in Fig. 3.

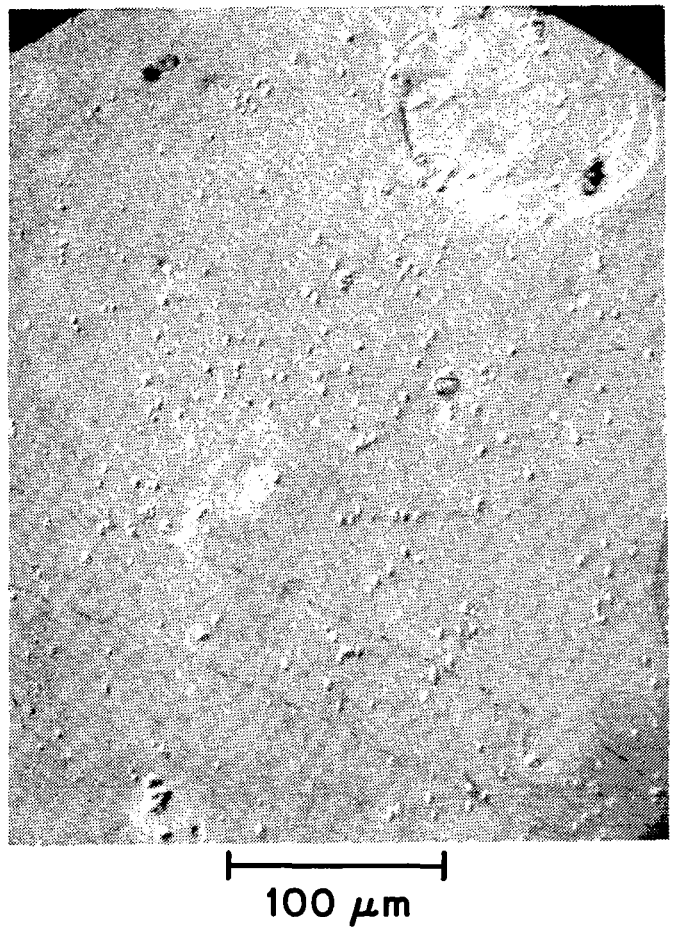

Figure 3. Individual etch pits are easily resolved and correspond to areas where dislocations make steep angles with the surface.

B. PULLOVER

It is well known that there can be irregularities in the growth of multiple layers by LPE. For example, there are occasional variations in the emission wavelength of AlGaAs devices caused by fluctuations in the aluminum concentration in the melt. These fluctuations can occur because of the sensitivity of aluminum dissolution to the residual oxygen content in the furnace, or to other causes such as pullover of

200 μm

Figure 4. X-ray topograph (400/Mo) of typical InP wafer used in this work.

material from an earlier bin in a multiple bin boat. It is also possible that meltback of a previously grown layer may occur when the wafer and a new melt are brought into contact, a situation considered highly probable by some authors [3]. Growth disturbances also occur in the InGaAsP/InP system, and in a recent paper [4] these have been attributed to meltback of the active layer. InGaAsP is especially suitable for a study of this problem because the layers surrounding the active layer, the cladding layers, normally contain only In and P, so that any contamination by Ga and As can be easily detected. In the AlGaAs system such measurements are more difficult since all three elements occur in every layer.

In the present section we examine a type of growth disturbance occasionally seen in InGaAsP/InP 1.3-μm LPE grown material, and we attempt to elucidate its origin. Arguments will be presented to show that the disturbance is attributable to pullover and that there is no evidence for meltback in the samples studied.

The material was grown in a standard multiple bin boat, using the two-phase technique [5]. In particular, the melt was initially equilibrated by heating for one hour at 675°C and then cooled at 0.5°C per minute. At 655°C the wafer was first exposed to the melt, and the active quaternary layer was grown at 635°C. The total weight of the melt was 4.4 gm and the area of the wafer was 1.3 cm^2. In two-phase growth there is competition between the growth on the substrate and growth on the InP wafer placed on top of the melt. Nevertheless, the melt is believed to be supersaturated in the vicinity of the growth interface [6].

The main observed effect is the occasional production of a wafer whose surface appearance is not noticeably different, but which has a high threshold current and which presents an unusual X-ray diffraction pattern.

For purposes of illustration in what follows, two wafers are analyzed which typify these observations. One is the so-called "anomalous" wafer, and the other is a "normal" wafer grown identically, as nearly as possible, but which shows a standard X-ray pattern, and which is normal in other respects also.

In the X-ray diffraction experiments either shallow (2 μm) or deep penetration (10 μm) of the X-ray beam can be selected [1] by the choice of diffracting planes (angles of incidence). Referring to Fig. 5 which indicates typical layer thicknesses in our laser material, the shallow penetrating beam can be seen to sample the material from the surface to the active layer, whereas the deeply penetrating beam also includes most of the n-InP cladding layer.

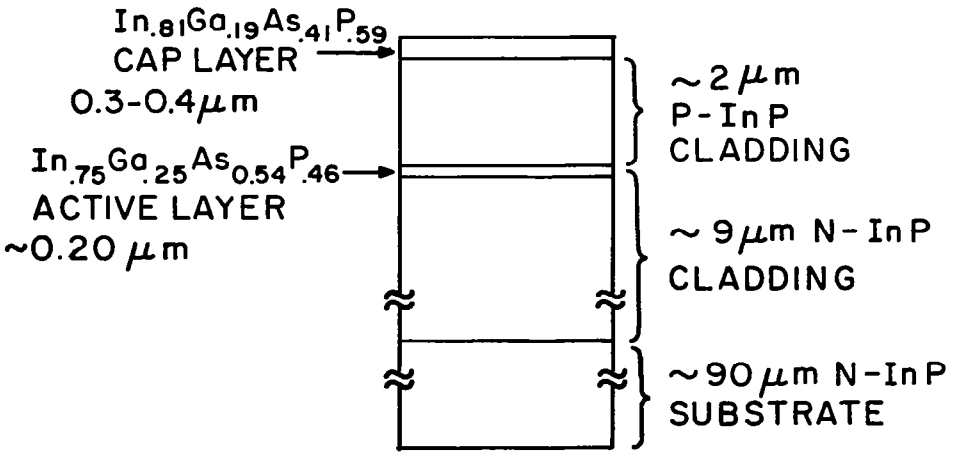

Figure 5. Schematic indicating layer thickness and the composition of the active and cap quaternary layers.

Shallow and deep penetrating cases are shown for the anomalous and normal samples in Figs. 6(a) and 6(b), respectively. In both cases, the quaternary cap was removed by etching in H_2SO_4:H_2O_2:H_2O. In Fig. 6(a) it can be seen that there exists a phase which is mismatched with respect to InP. In the shallow penetrating case (440 reflex) of this figure, only the mismatched phase is observed. Since in this case beam penetration is limited to the top 2 μm which includes mostly the p-type cladding layer, it can be concluded that this layer has a lattice-constant different from that of InP and is therefore not composed of pure InP.

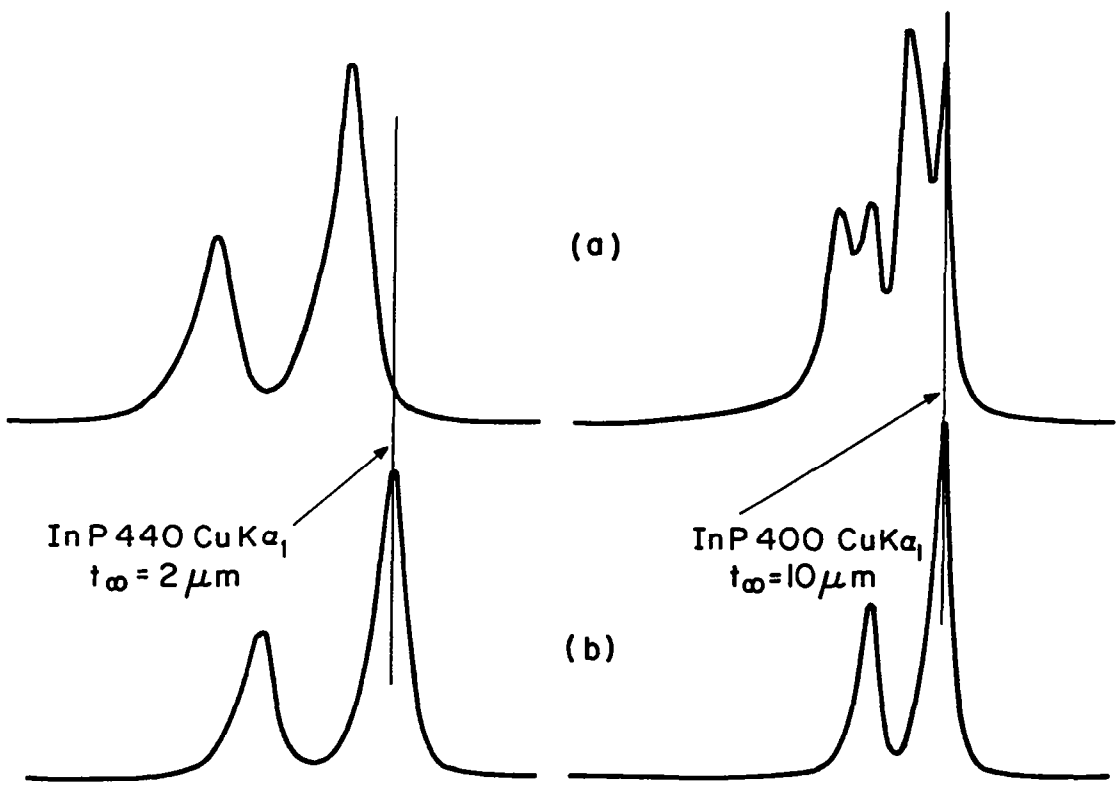

Figure 6. X-ray diffraction patterns of the (a) anomalous and (b) normal wafer. The quaternary cap layer was removed by etching before these patterns were taken.

The mismatch from InP shown in Fig. 6(a) is +0.1%, which yields a lattice constant $a^* = 5.8665$, after the tetragonal distortion correction is applied [7].

Photoluminescence (PL) spectra of the anomalous wafer were taken with the topmost quaternary layer etched off (trace I in Fig. 7) and with most of the p-type cladding layer also etched off (trace II in Fig. 7). In case I the room-temperature peak occurs at 0.934 μm, and in case II the peak occurs at 0.920 μm. These values are typical for room temperature PL of our normal layers grown by LPE where the peak for p-type InP occurs at 0.932 to 0.934 μm, and for n-type InP at 0.918 to 0.920 μm. They are also in reasonable agreement with the data published by Onton et al. [8]. The bandgap of the cladding material on both sides of the active layer is, therefore, not appreciably different from that for pure InP. However, the +0.10% mismatch on the p-side indicates a change in lattice constant as mentioned before, from which one can deduce [9] that the composition of the p-cladding is $In_{.9904}Ga_{.0096}As_{.0057}P_{.9943}$.

Both samples were analyzed by secondary ion mass spectrometry (SIMS) in order to obtain a depth profile. Figures 8 and 9 show profiles through the anomalous wafer and through the normal wafer, respectively. The depth coordinate which corresponds to layer thickness measured from the surface was obtained by calibration of the sputtering rate with a sample of pure InP. Taking the counting rate as a linear function of the atomic concentration of each element and using the composition of the active layer obtained from photoluminescence measurements as a calibration point for each of the elements, one obtains values for the atomic fractions of Ga and As in the p-cladding.

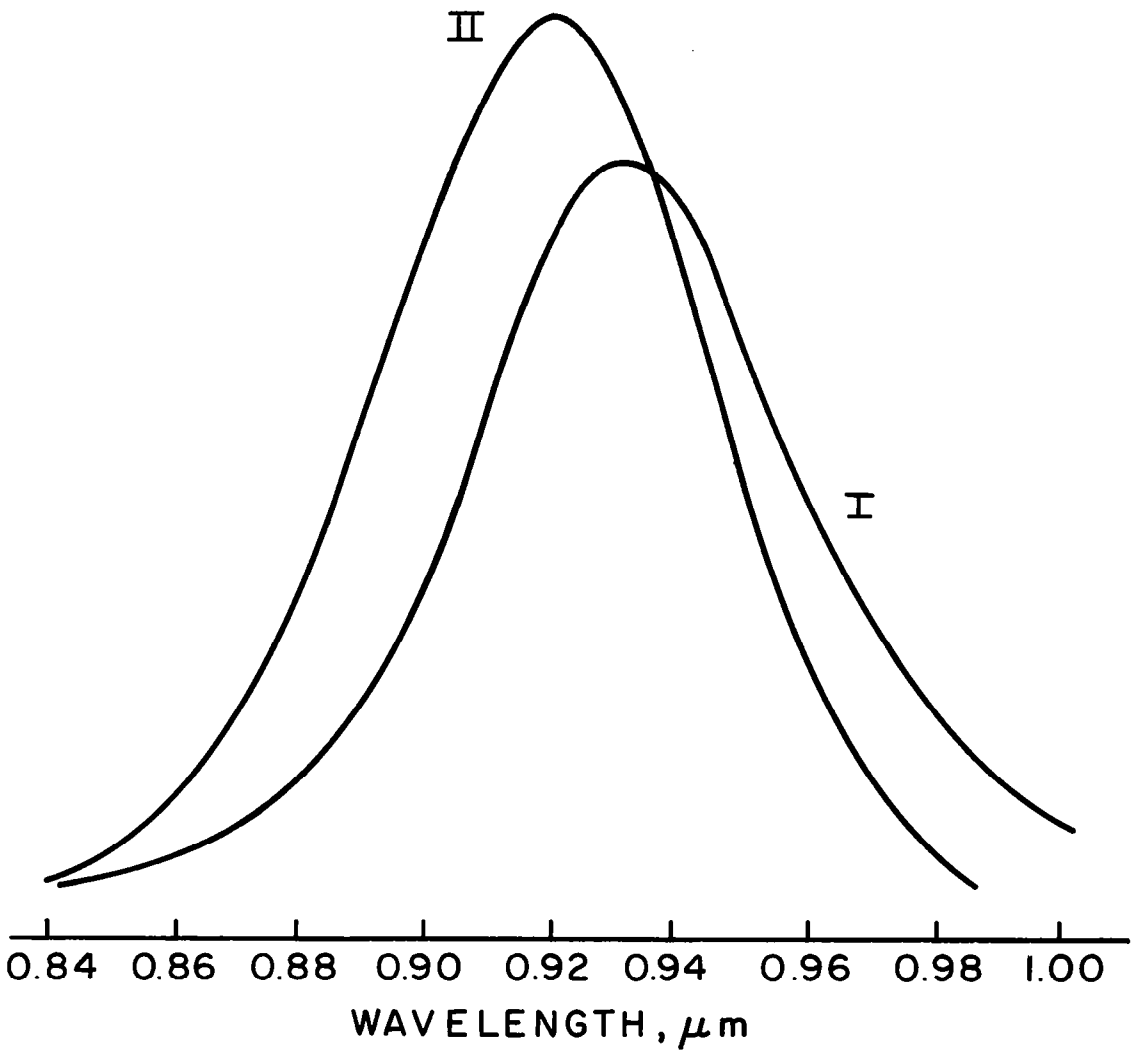

Figure 7. Room-temperature photoluminescence scans using argon-ion laser excitation. Trace I is obtained from the anomalous wafer after the quaternary cap layer is removed. Trace II results when the p-type cladding layer is also removed.

Although the concentrations involved here are near the limit of sensitivity for electron probe microanalysis (EPMA), the two samples have been analyzed by this method using GaAs as a calibration standard.

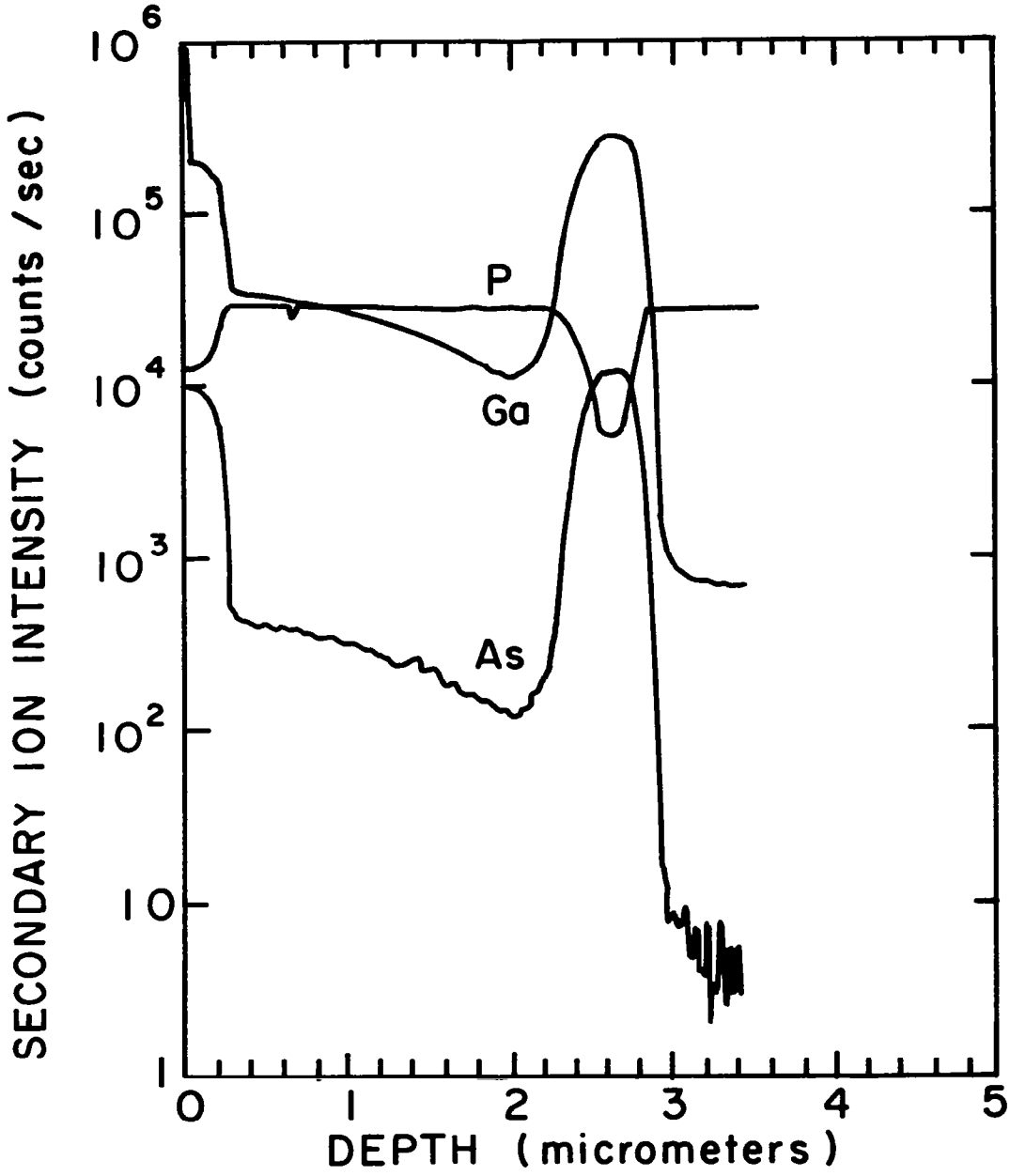

Figure 8. SIMS profiles through the anomalous wafer.

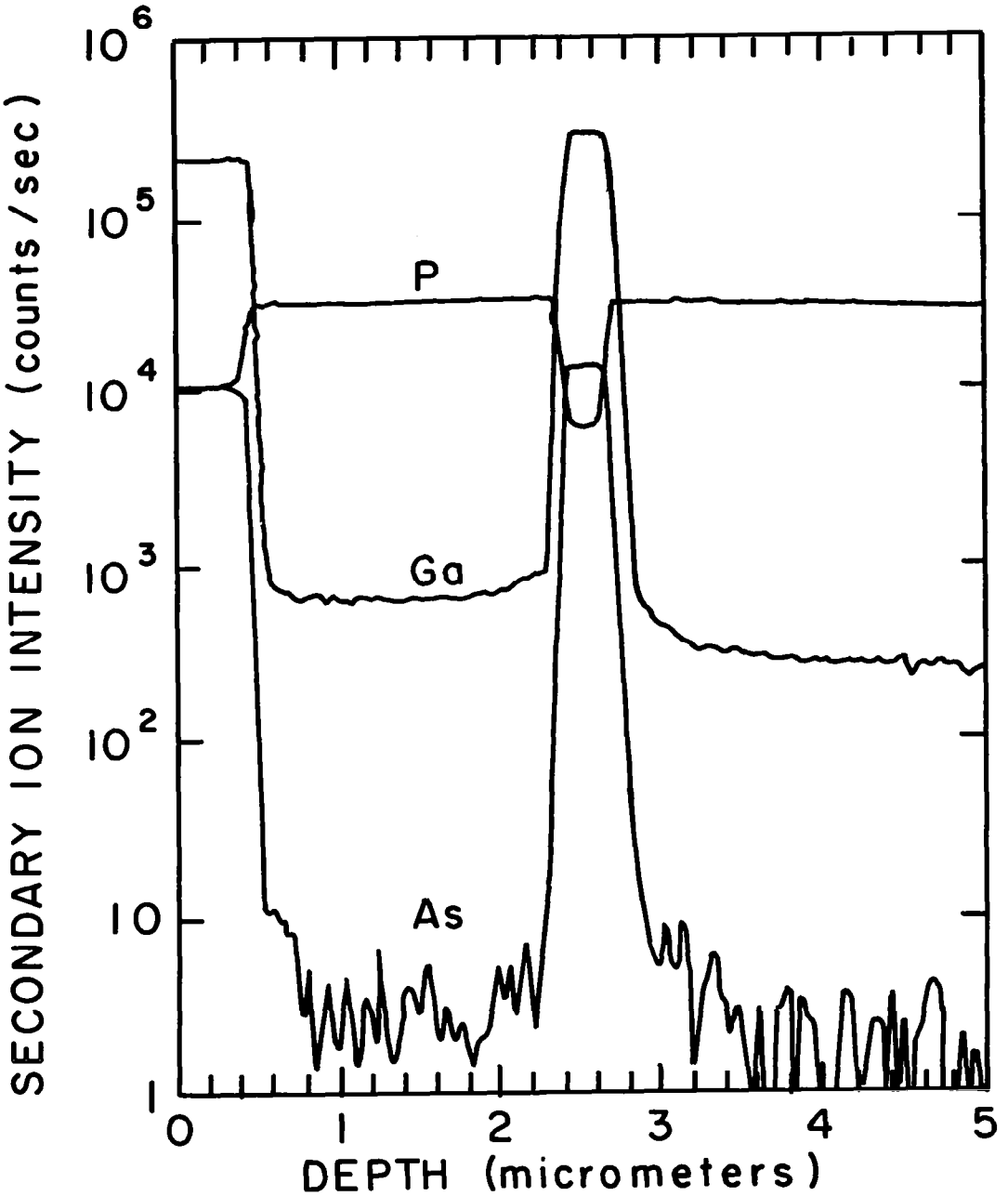

Figure 9. SIMS profiles through the normal wafer.

Table 1 summarizes the analytical results. The term atomic fraction when applied to the solid means the atomic fraction in the Group III or Group V sublattice.

TABLE 1. SOLID COMPOSITION IN P-CLADDING LAYER OBTAINED BY VARIOUS METHODS

Atomic Fraction Ga			Atomic Fraction As		
From PL and a*	SIMS	EPMA	From PL and a*	SIMS	EPMA
0.0096	0.01-0.03	0.012	0.0057	0.005-0.02	0.010

Using PL and the lattice constant, a composition has been determined for the p-type cladding layer which seems to be in good agreement with values obtained by SIMS measurements. SIMS profiles, furthermore, indicate that the composition varies through the p-cladding layer. Comparing Figs. 8 and 9, the active layer in the disturbed sample is seen to be wider, with a tail reaching into the p-cladding, and the As and Ga concentrations first decrease and then both rise toward the cap layer. This behavior can be understood if one assumes that some melt had been pulled over from the previous bin. If this melt enters as a film adhering to the wafer surface, a gradually decreasing Ga and As concentration could ensue. Their subsequent rise indicates a further increase in these elements, such as would result from the presence of a new source, perhaps due to a communicating channel with the previous bin. Alternately, some of the pulled over melt may have been stirred into the new melt, providing a gradually increasing source of Ga and As.

The question considered next is whether a plausible explanation for the SIMS profiles can be advanced assuming meltback to be the source of the contamination. After dissolution of some fraction of the active layer, the newly grown material would initially have a composition somewhat different from that of the active layer. Subsequently,

because of the dilution of material, the As and Ga concentrations would decrease. It is difficult to see how an increase can be obtained without bringing in a new source of As and Ga, and the width of the active layer would also have to show a reduction, rather than an increase. SIMS profiles, therefore, exclude meltback and are not inconsistent with pullover as the source of contamination.

It is possible to estimate the quantity of melt pulled over from the preceding bin which is needed to produce the observed solid composition. Using for this purpose the segregation coefficients for Ga and As, defined as [5] $1k_{Ga} = x/2X^{\ell}_{Ga}$; $k_{As} = y/2X^{\ell}_{As}$ and previously published data for two-phase growth [8], one obtains a series of k values shown in Fig. 10, together with the straight line extrapolation presented by Pollack et al. [5]. It will be seen that there is substantial agreement between these two sets of data, suggesting that the published extrapolations for y = 0 should be valid for the present work as well. From $k_{As} = 4.2$ and $k_{Ga} = 34$ one obtains $X^{\ell}_{Ga} = 0.00014$ and $X^{\ell}_{As} = 0.00068$ for the liquid concentrations in the p-cladding melt. The melt used to grow the active region has [8] $X^{\ell}_{Ga} = 0.0087$ and $X^{\ell}_{As} = 0.049$, so that a dilution by a factor of 62 for Ga and 72 for As is required. These two values are in reasonable agreement, considering the uncertainty in the distribution coefficients. A mean dilution of 66 implies that 67 mg of InGaAsP growth solution was pulled over from the 4.4-gm melt.

Wafers with p-cladding X-ray splitting corresponding to 0.1% lattice mismatch generally have a broad area threshold current density in the 7- to 10-kA/cm^2 range, whereas those showing a splitting which is less than 0.08% have a threshold current density in the 1.5- to 2.4-kA/cm^2 range, the value reproducibly observed in normal wafers.

The refractive index of InGaAsP mismatched from InP by 0.1% has an index within 0.002 of that for pure InP[6] and is, therefore, not likely to interfere with optical confinement. The increase in threshold current density is more likely due to reduced injection levels caused by interface recombination or carrier confinement difficulties.

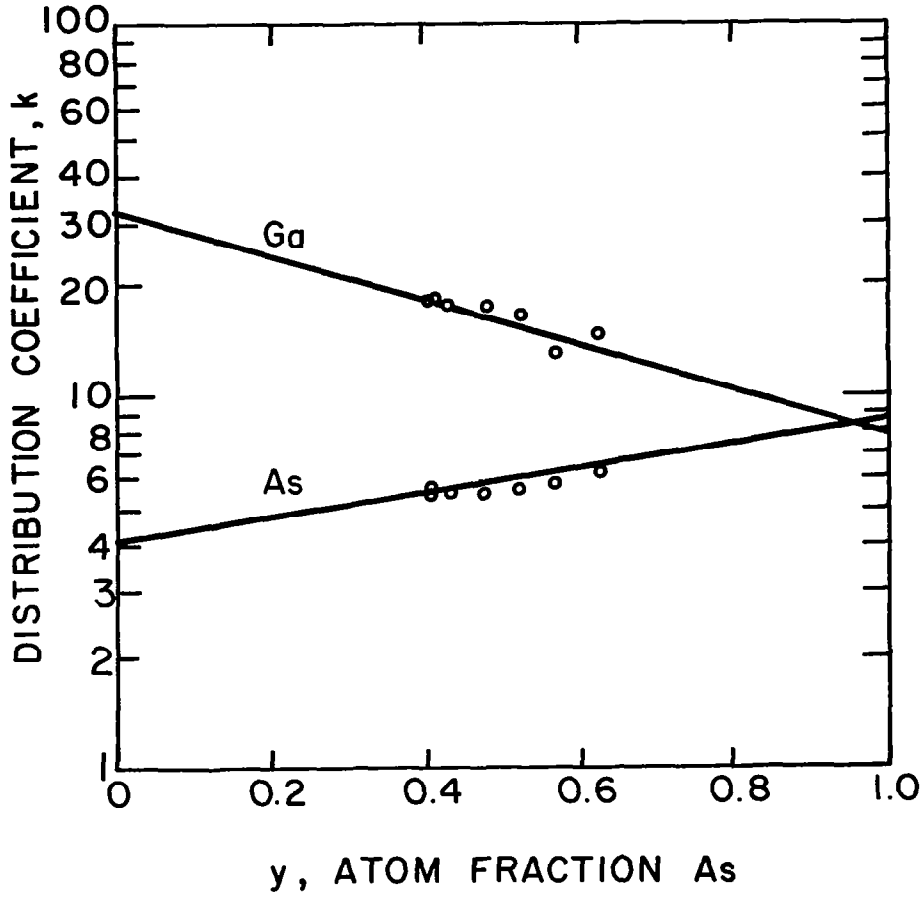

Figure 10. Experimental values for the distribution coefficients. Solid lines shown extrapolated values of reference 3.

Nothing has been said so far about the reasons why these disturbances occur. There might be an occasional malfunctioning of the boat in which the layers are grown. In common with most sliding boat designs, the degree to which the melts are separated depends on the gap left between the surface of the wafer and the boat partitions separating the various melt-containing bins. In our apparatus this gap is maintained at a fixed value of 0.01 cm, and it is not easy to see how this

can change. Second, one might suppose that a property of the substrate is involved that controls the adhesion of the melt to the wafer surface. Such a possibility is suggested by the angle lap photomicrographs shown in Fig. 11, which compare the normal wafer (a and c) to the anomalous wafer (b and d). The comparatively larger steps (b and d) shown at the boundaries between the cladding and the active layers might, in this model, assist in transferring the solution when the substrate is advanced to the next bin. However, this effect is not seen in every case nor in the majority of cases, and must therefore be a coincidence. Measurement of the surface orientation performed on the two wafers shows that both are oriented to the (100) plane within 0.3 to 0.4°, the difference in their orientations being 0.08°. Thus, it is not likely that there are any significant effects associated with wafer misorientation. Factors such as differences in dislocation density or other structural parameters cannot be ruled out at present.

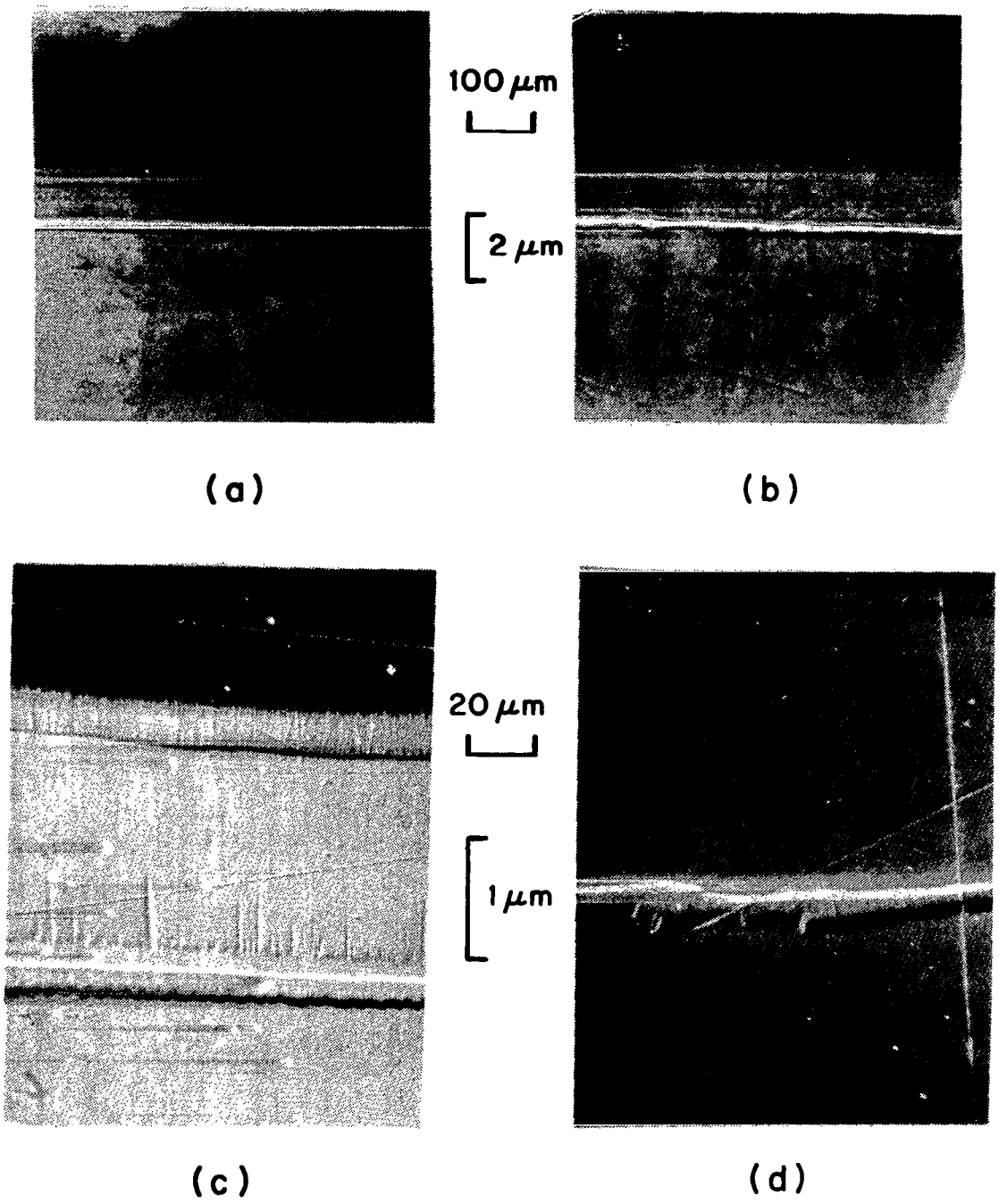

Figure 11. Angle lap photomicrographs through the normal (a and c) and the anomalous (b and d) wafers.

II. GENERAL DEVICE STUDIES

A. ACCEPTOR DOPING

Two types of acceptors have been used in the course of this work, zinc and cadmium. The basic problem concerning these dopants is that they are volatile and thus may change in concentration and contaminate other melts. Some evidence of this occurring was observed, and we therefore preferred to use the aliquot method of introducing dopants into the melt. A certain quantity of dopant is first dissolved in In and some part of this alloy is used to dope the melt. By this means the dopant loss is largely eliminated. However, due to lack of reproducibility in threshold current density mentioned earlier, we decided to investigate the In/Zn alloy with a nominal composition of 2% Zn. A slice of this alloy was cut from the ingot and subjected to chemical analysis using atomic absorption spectroscopy as well as spatial sampling by means of Energy Dispersive X-Ray Analysis (EDXRA). A photograph of the sample is shown in Fig. 12 which also shows the EDXRA count ratios and the result of the chemical analysis in two different areas. For a uniform alloy composition the count ratios would be constant, and the analysis would yield a fixed value of 2%. It is seen that the ratios are extremely variable, not only across the slice, but also in adjacent regions, and that the average chemical analysis varies by a factor of three for the two portions of the slice. In order to explore these variations further, we have repeated the EDXRA analysis at high magnification (Fig. 13) and mapped the results in such a way that wherever the zinc signal was above a preset limit, a white dot would be produced on the cathode ray screen. Comparing the EDXRA dot map with the secondary electron image, considerable similarity is observed, indicating that there are topographical features which correlate with the zinc signal. The bottom figure taken at the higher magnification SEM shows small spherical globules which appear to be composed principally of zinc, as shown by comparing the EDXRA signal with the corresponding spot as indicated by letter. Zinc in this alloy

In/Zn SAMPLE

NOMINAL
COMPOSITION: 2% Zn

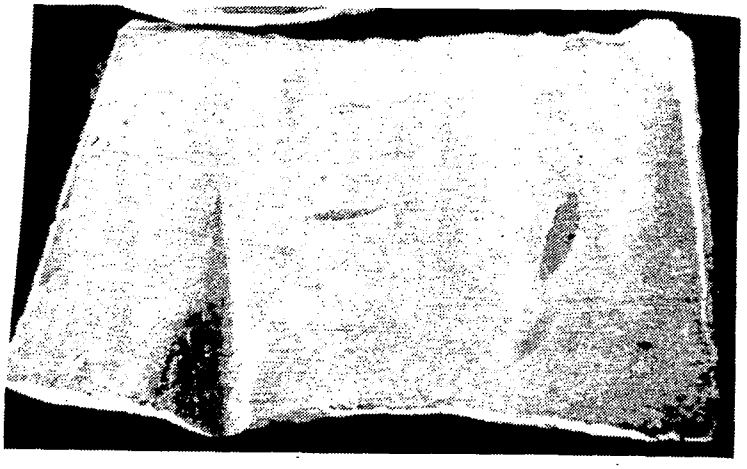

EDXRA

Zn:In
COUNT RATIOS

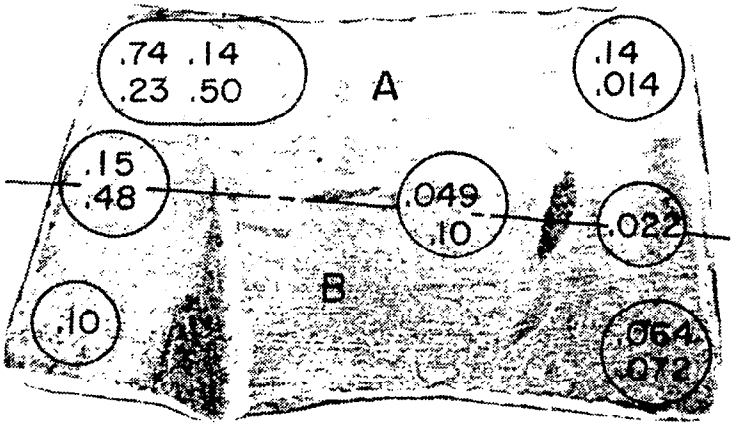

ATOMIC ABSORPTION ANALYSIS

A 3.1% Zn
B .93% Zn

Figure 12. In/Zn alloy used for acceptor doping. Upper part of the figure shows the slice of material used in the analysis, and the lower part of the figure shows the points where EDXRA counts were made and the corresponding count ratios for Zn/In. A uniform composition would yield a constant ratio. Result of atomic absorption analysis for the two pieces of material separated along the dotted line shown at the bottom.

EDXRA STUDY OF Zn/In ALLOY

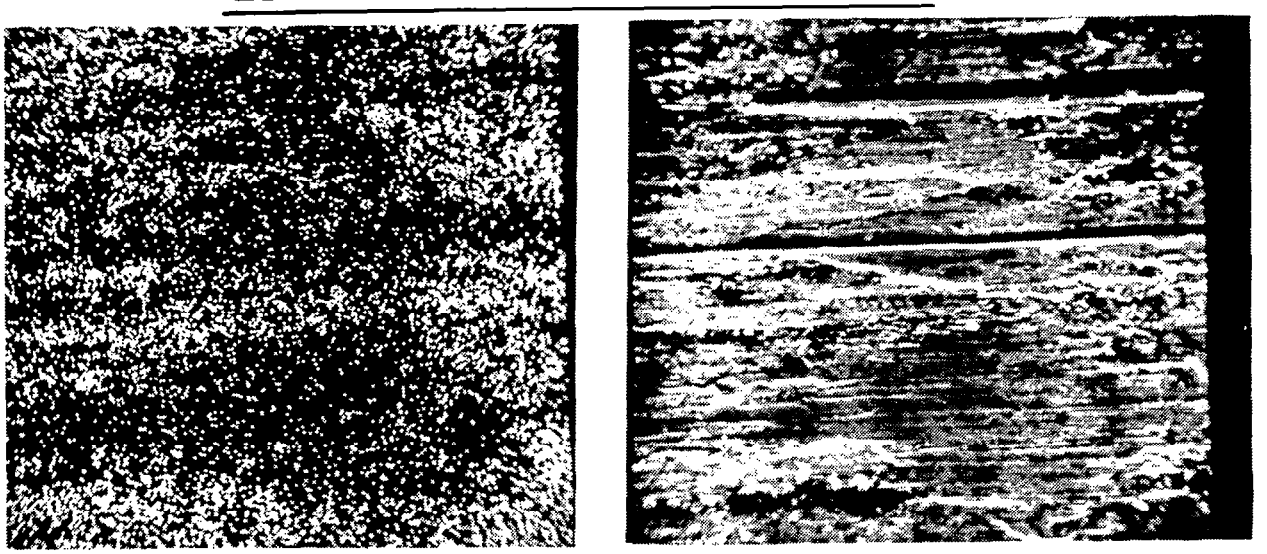

DOT MAP-Zn COUNTS - 25μm SEM

(a)

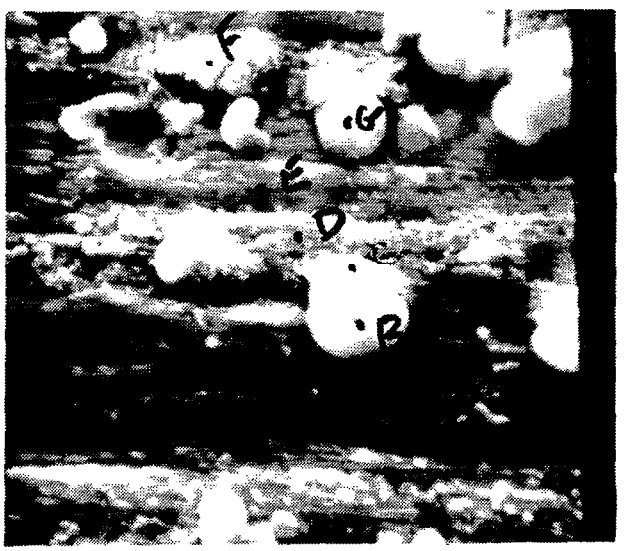

SEM 2.5μm

(b)

LOCATION	$\frac{Zn\ (K\alpha)}{In\ (L\alpha)}$ X-RAY INTENSITY RATIO
A	0.008
B	3.3
C	0.8
D	0.3
E	0.02
F	1.3
G	2.8

Figure 13. (a) Dot map showing distribution of Zn and corresponding SEM image of section of nominal In-2% Zn alloy. (b) Higher magnification SEM of same specimen. It can be seen that globules (marked B, F, G) give higher Zn/In x-ray intensity ratios and intermediate areas give low ratios.

appears to segregate so that a uniform doping source cannot be expected from its use. However, when a source with one-tenth the Zn concentration (0.2%) was made, atomic absorption analysis showed a uniform concentration for different portions of a sample, and EDXRA did not reveal any zinc segregation. Thus, a concentration of 2% exceeds the solubility of zinc in In and a concentration of 0.2% is under the solubility limit. We now use the lower concentration alloy exclusively, which has resulted in more reproducible threshold current densities.

B. EBIC MEASUREMENTS

In order to locate the pn junction in grown materials, we have examined a number of structures using the scanning electron microscope in the Electron Beam Induced Current (EBIC) mode. Figure 14 illustrates the type of result obtained. Each part shows the active region of a specimen, with line traces for the secondary electron and EBIC signals superimposed on the SEM image. In each micrograph, the nominally n-type cladding layer is on the left side, the cavity is visible in the middle, and the p-type cladding is on the right. The straight horizontal trace indicates the scan line along which the analysis was made. The EBIC trace is sharply peaked in the region near the cavity layer. Figure 14(a) shows two EBIC curves: The upper trace was taken with relatively low amplifier gain to show the general shape of the EBIC profile; the lower EBIC trace (which is actually the same curve) was photographed with higher amplifier gain and zero suppression in order to show only the peak of the EBIC curve. The EBIC traces in Fig. 14(b) and (c) similarly are shown highly amplified and zero suppressed. The broad, noisy trace is the secondary electron signal which is used to show the boundaries of the active layer. This trace is displayed to facilitate an accurate correlation of the physical structure with the EBIC signal. It can be seen that the secondary electron signal profile agrees well with the position of the etch-delineated cavity.

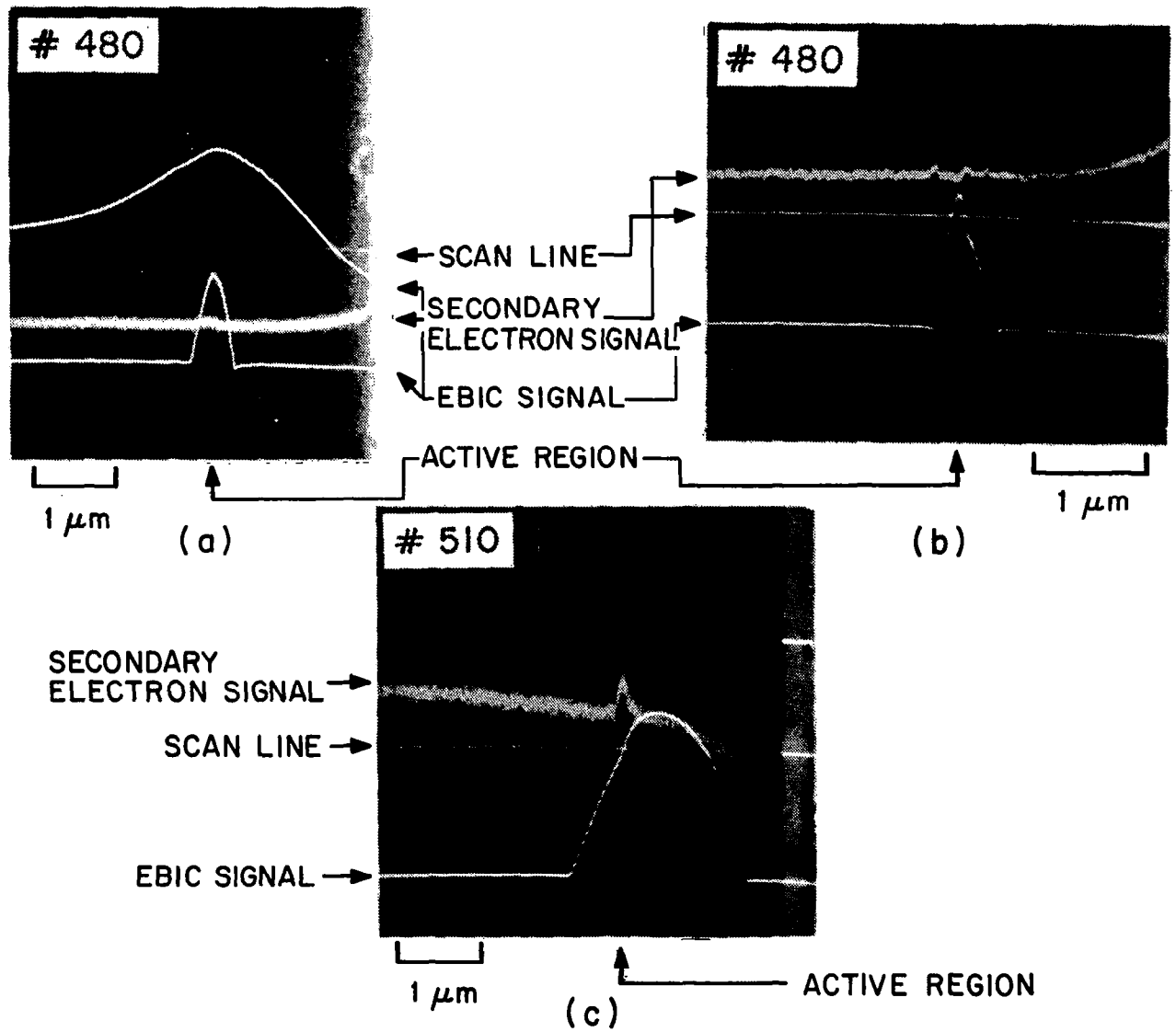

Figure 14. EBIC scan of two Zn-doped samples (#480) and of one Cd-doped sample (#510). The location of the junction, taken to be at the peak of the EBIC signal, is seen to be in different regions of the structure.

The initial assignment of junction position is made tentatively, according to the growth program; however, the junction may be displaced from this position, depending on the actual impurity distribution present in the layers. Figure 14(a) shows an unetched specimen from a wafer in which Zn was used as the p-dopant; Fig. 14(c) is an unetched specimen with Cd as the p-dopant. The junction location is taken to correspond to the peak of the EBIC signal. In the Zn-doped material (a), the junction appears near the middle of the active layer, while in the case of Cd doping (c), the junction is clearly outside the active region, in the p-type cladding layer.

Another interesting observation is demonstrated by comparing Figs. 14 (a) and (b), which differ in having the active layer delineated by etching (b) or being unetched (a). The junction position as indicated by EBIC seems to depend on the presence or absence of etching: In (b), the junction appears to be at the boundary between the cavity layer and the p-type cladding; in (a), as noted above, it is inside the cavity layer. This apparent shift is an effect of the topography introduced by the etching. Consistent results can be obtained if samples are always examined with no or very light etching.

The significance of the junction position is made apparent by the following observation. Two wafers, both grown with Cd as the p-dopant, were examined by EBIC, and the broad area threshold currents were measured. The pn junction was located inside the p-type cladding layer, at the position indicated in Table 2.

TABLE 2. JUNCTION POSITION MEASUREMENTS

Average Junction Position From Edge of Active Layer (μm)	Threshold Current Density (kA/cm^2)
0.1	4
0.35	9

Not surprisingly, a junction position not close to the active layer implies carrier loss and high threshold current.

The position of the junction is clearly not controlled since no deliberate attempt was made in this experiment to locate it in different positions. For this reason and because of the appreciably higher vapor pressure, we have not pursued Cd doping experiments to any great extent. It is possible to conclude that some failures in obtaining reasonable threshold currents are caused by junction displacement resulting from poor control of impurity levels.

C. OHMIC CONTACT TO P-SIDE

Zinc is also used in the p-type device contact. In our work Au/Zn alloy is evaporated onto the material and sintered at an elevated temperature. Attempts to determine the depth of zinc diffusion during this process showed that zinc did not spread below the depth of Au penetration. We may, therefore, assume that the depth to which zinc penetrates in this contact is equal to the depth to which gold penetrates. In order to obtain some information about the depth to be expected, we have analyzed several samples by secondary ion mass spectrometry (SIMS). Figure 15 shows SIMS profiles obtained. The As signal is taken as the measure of the layer thickness, typically 0.4 μm, from which a calibration of the horizontal scale in terms of depth can be obtained. Results are given in Table 3. The Au penetration in the first two cases is negligible and largely determined by instrument bias, but for the 400°C sintering indicates a depth of 0.13 μm. Thus, our present contact technology produces a Zn and Au penetration to a distance which appears sufficiently small to preclude affecting the device performance (something which could be expected to happen if the contact materials were to penetrate into the p-cladding region).

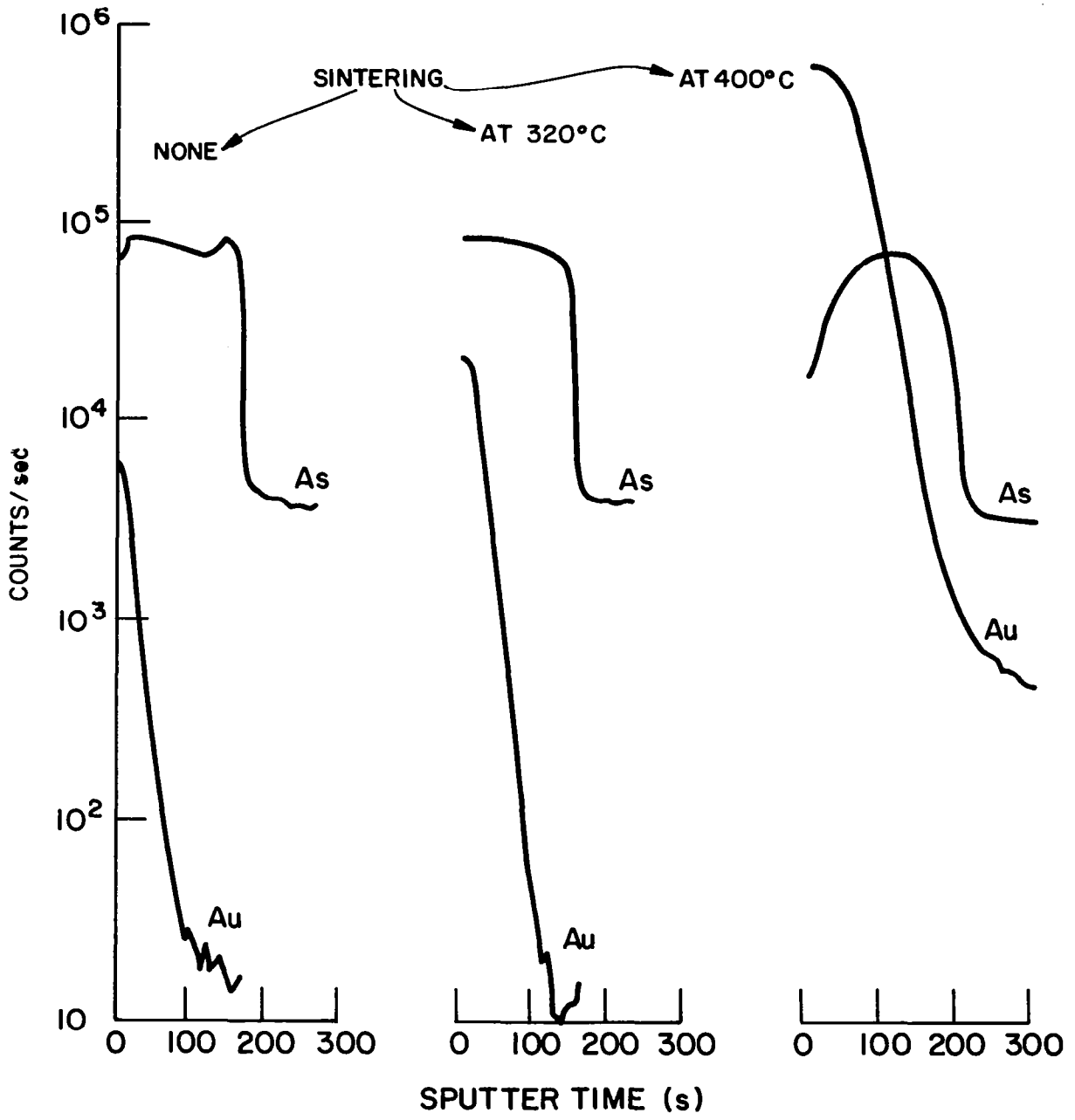

Figure 15. SIMS profiles through the ohmic contact to the p side of a typical device. As and Au profiles for no sintering and for two different sintering temperatures are shown. Gold was removed from the surface of unsintered and 320°C sintered samples prior to analysis.

TABLE 3. RESULTS FROM SIMS PROFILES

Contact Sintering Temperature (°C)	Depth of Au (Half Count) (μm)
none	0.05
320	0.06
400	0.13

D. MINIMUM THRESHOLD CURRENT DENSITY

Part of the objective of this contract was to reduce the threshold current density of broad area devices below the value obtained in the previous contract which was in the neighborhood of 1500 A/cm^2. The lowest achievable threshold current density is a quality factor, in that by achieving low values, a certain control is demonstrated over the parameters important for laser performance which allows for the development of the more advanced single-mode structures. Figure 16 shows broad area threshold current densities obtained for one particular wafer grown in this program. For these devices, the length to width ratio was made at least equal to 3, in order to reduce the probability of cross or internal lasing. A threshold current density of 1000 A/cm^2 is shown for the longest devices tested, L = 1080 μm. It is to be noted that the plot of J versus 1/L is not a straight line, as expected from theoretical considerations. As is well known [1], the threshold dependence is given by an equation of the form,

$$J_{th} = C_1 \left\{ C_2 + \frac{C_3}{L} \right\}$$

and other investigators have reported that their experimental results do not lead to any deviations from this dependence. In fact, not all

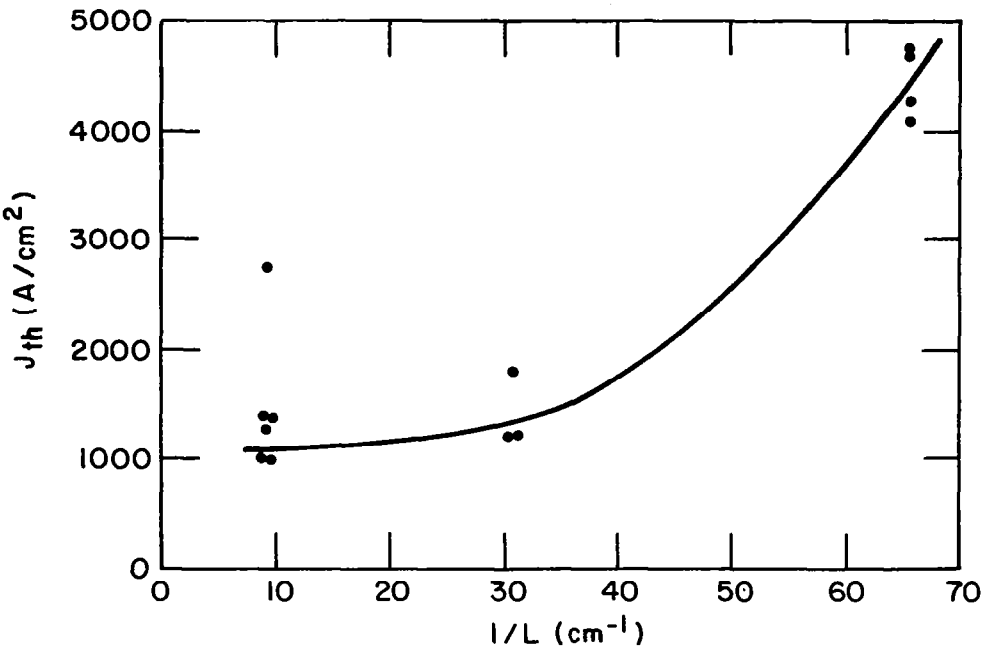

Figure 16. Threshold current density versus length for low threshold material.

wafers made here show this discrepancy. In the past such deviations have been blamed on cross lasing or internal lasing [10]. Examination of the spectrum of one of the short lasers shows no evidence of internal lasing.

In order to obtain the lowest threshold current densities, it is necessary to reduce the p-type doping level. We find, in agreement with other laboratories, that J_{th} decreases as doping is reduced. This appears reasonable, since it is well known that various nonradiative processes, such as Auger recombination, free-carrier absorption, etc.,

increase in probability as doping increases. The difficulty is that as one attempts to reduce the zinc concentration, the residual impurities become more significant, and can in fact establish the pn junction far from the desired position as discussed in an earlier section.

III. SINGLE-MODE LASER DEVELOPMENT

A. GENERAL APPROACH TO SINGLE-MODE LASER FABRICATION

There are by now a large number of single-mode laser designs described in the literature so that if one is faced with the task of developing a single-mode laser, the choice of structure to be used becomes a difficult problem. Different considerations arise if one wishes to maximize the yield of devices. Thus, a structure which may be desirable in one laboratory may actually be less so in another; there is also the possibility that authors are reluctant to describe all their difficulties. For all these reasons, we decided to approach the development of single-mode lasers in the InGaAsP system in as systematic a way as possible.

Injection laser devices can be classified according to whether they obtain their spatial characteristics through gain guiding or through index guiding. In the present work we deal only with index-guided structures because of their various advantages, such as the absence of astigmatism, linearity, single-mode output, etc.

Lasers can also be classified from the point of view of fabrication: devices grown in one step and devices grown in two steps, depending on whether all the growth occurs in a single LPE growth cycle or in two such cycles. In Fig. 17 we give one example for each type, recognizing that many others are possible. Figure 17(a) shows a one-step device, a constricted double heterojunction (CDH) type. Here a double groove is etched into the substrate, and the LPE layers are all grown in a single step afterward. An advantage of this process is that exposure of any critical surface to ambient air or high temperatures is avoided, this being beneficial in regard to life. The disadvantages of this method are that the growth has to be tailored to the groove structure used, that it depends on orientation, and that it is not necessarily repeatable in different materials (i.e., AlGaAs vs InGaAsP).

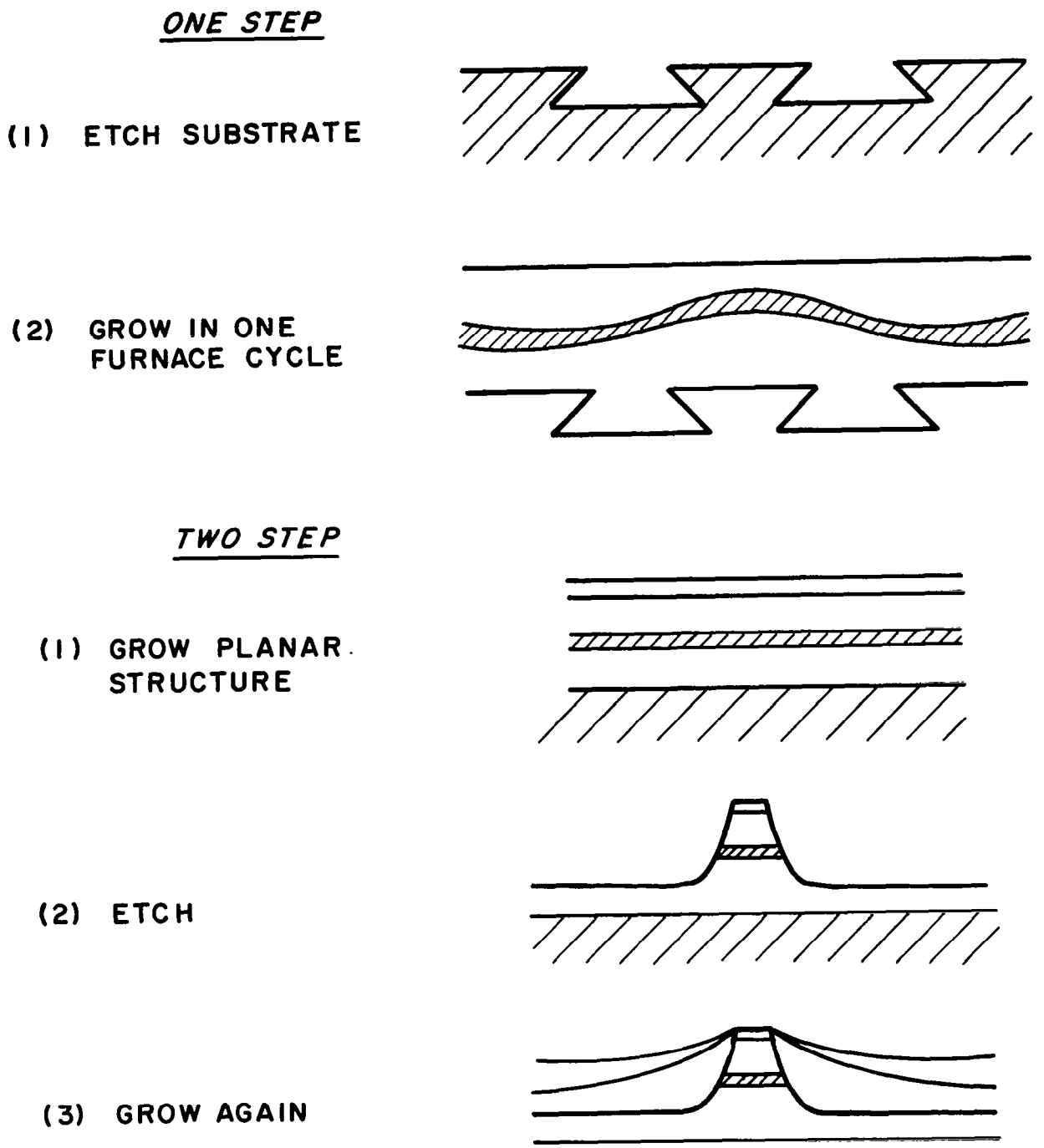

Figure 17. Examples of one-step and two-step growth of index-guided material.

Figure 17(b) shows an example of a two-step structure, a buried heterostructure (BH) laser. Starting with a planar four-layer wafer, the mesa is etched first, and the structure is next subjected to another LPE growth cycle during which the sides of the device are filled in. The advantage is that a good wafer can be selected, and that the growth is well understood and controlled. The disadvantage is that surfaces in the vicinity of the active layer are exposed to ambient air, and that the original layers are subjected to another heat cycle with possibly undesirable consequences.

In any case, the majority of single-mode structures will during the fabrication cycle require growth over some kind of nonplanar surfaces such as grooves or mesas. It is thus possible to develop a further classification of devices, based on the type of surface used as a substrate. For wafers oriented in the (100) plane, there are four possible grooves which can be obtained, depending on whether they are etched into the substrate or are made to rise above the substrate, and whether they are aligned in the [011] or the [0$\bar{1}$1] direction (Fig. 18). If one has information about how growth proceeds on these grooves, one should be able to construct any of the devices described or proposed in the literature. In the course of this work we have examined all of these grooves, with the following results.

1. Inverted V Groove

This is the configuration used to make CDH type lasers in AlGaAs. In the InGaAsP case, growth occurs on all surfaces to some extent but mostly on the (100) surface. Thus, we do not obtain a filling in of the etched cavity (Fig. 19). More meltback than was used here would be needed to obtain a configuration approaching that seen in the case of AlGaAs growth.

2. V Groove

Results, shown in Fig. 20, are very similar to the case above: slight growth on the inclined (111) surfaces and much more growth on

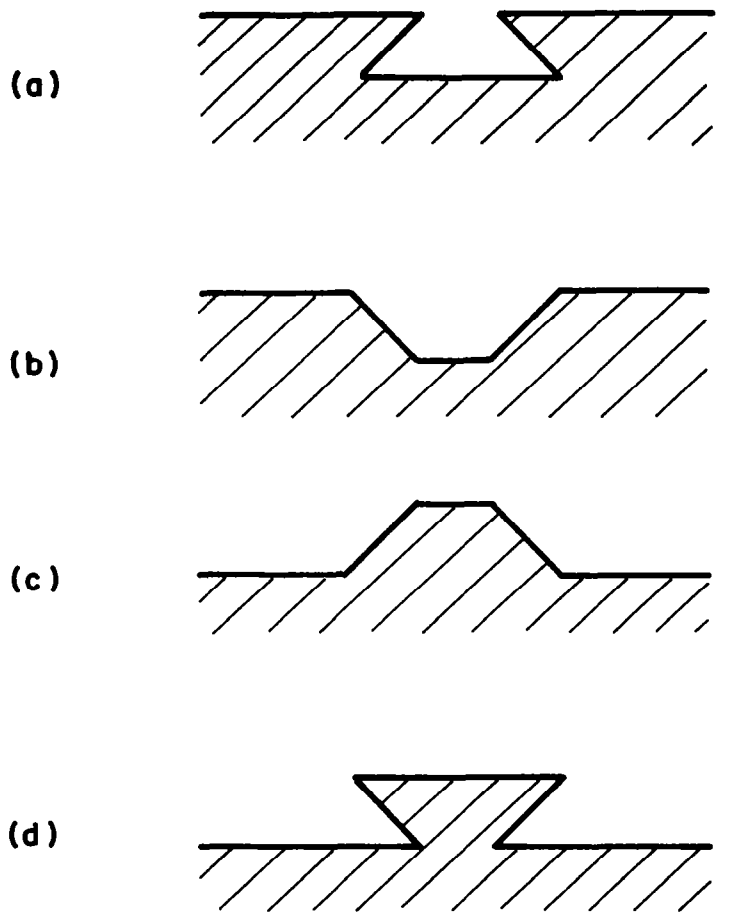

Figure 18. The four possible groove configurations for growth on the (100) plane. (a) Inverted V groove, (b) V groove, (c) inverted raised V mesa, and (d) raised V mesa.

the (100) surfaces. Again, no filling of the grooves occurs. This result, taken together with case 1 strongly suggests that these depressed grooves are not ideal for subsequent growth of conventional devices.

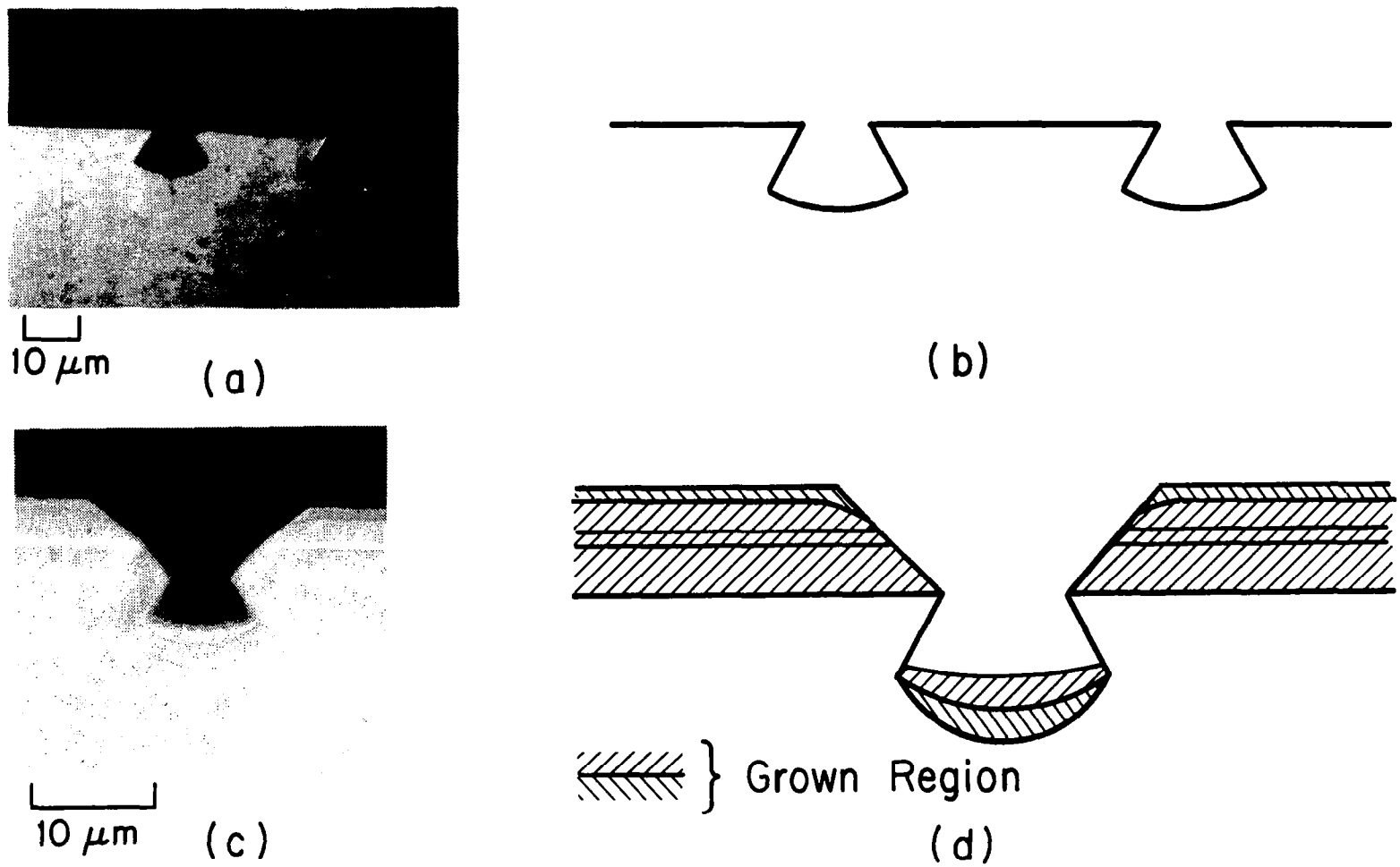

Figure 19. Growth on inverted V grooves. (a) Etched substrate, (b) schematic of etched pattern, (c) grown regions shown in optical photomicrograph, and (d) schematic of growth in (c).

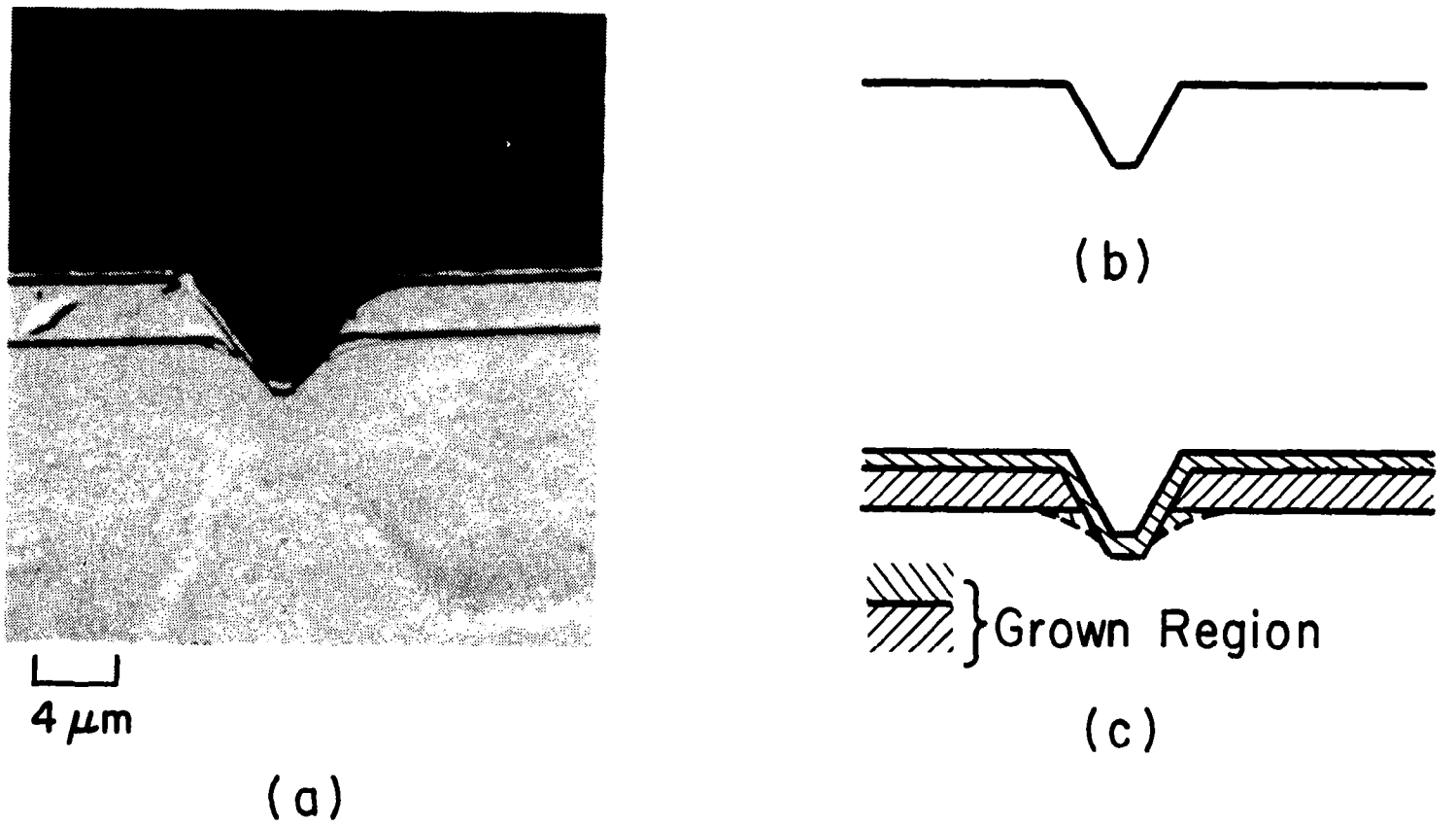

Figure 20. Growth in V grooves, showing (a) grown layer, (b) schematic of substrate, and (c) schematic of grown layers.

3. Raised V Mesa

This configuration is obtained by etching out thin stripes in a protected wafer and orienting the stripes in the [011] direction. As shown in Fig. 21, complete filling of the space on the side of the groove occurs, and furthermore, an active region is obtained which shows curvature and constrictions of the kind needed for mode confinement and control. Thus, this kind of stripe is suitable for various types of lasers, and its use should result in devices similar to those obtained in case 1 for AlGaAs. To our knowledge, no devices grown on this kind of mesa have yet been reported in the literature; part of our future program envisages exploration of this type of growth.

4. Raised Inverted V Mesa

Growth on this type of mesa has been used for the mesa stripe buried heterostructure (MSBH) laser as seen in Fig. 22. Filling is excellent, and a substantially planar surface was obtained. The cavity is clearly separated from the rest of the structure, giving the desired mode control.

To summarize this section, raised mesas have been found to be more suitable for laser growth in the InGaAsP system. This seems to be a consequence of the more rapid growth on (100) planes and slow growth on (111) planes. Under conditions of limited access by the melt, the available supply of diffusing species is rapidly depleted by growth on the (100) planes, and a void is left in some cases. Referring to Figs. 19 or 20, we see that the growth along an edge proceeds in such a manner that it assumes the (111) orientation. It is clear that for best growth one should arrange the structure in such a way as to take advantage of this natural geometry. The angle usually obtained for edge growth has the theoretically expected value of 54.7° (the angle between the (100) and (111) planes).

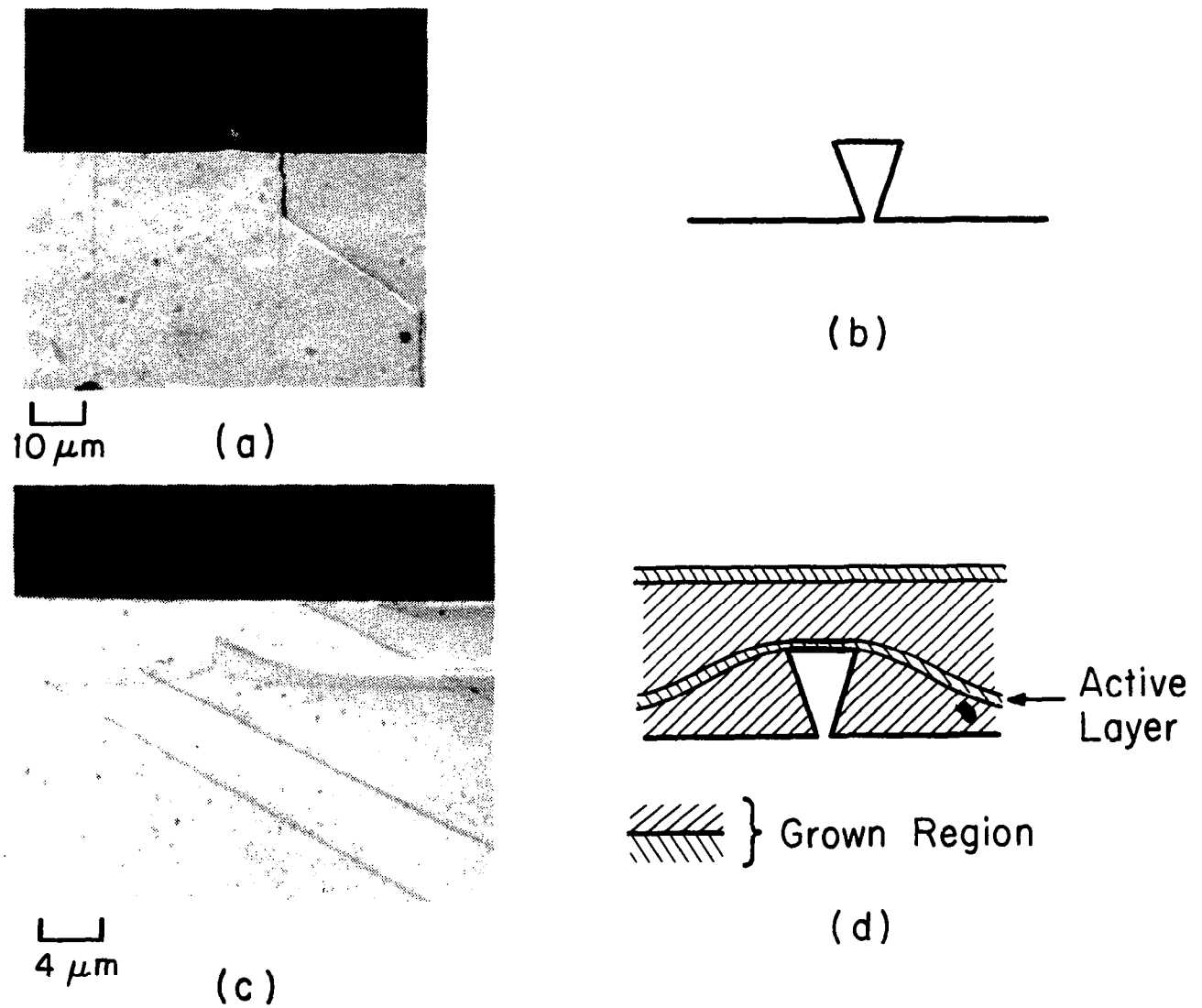

Figure 21. Growth on raised V mesa, showing (a) substrate cross section, (b) substrate schematic, (c) completed growth, and (d) schematic of grown layers.

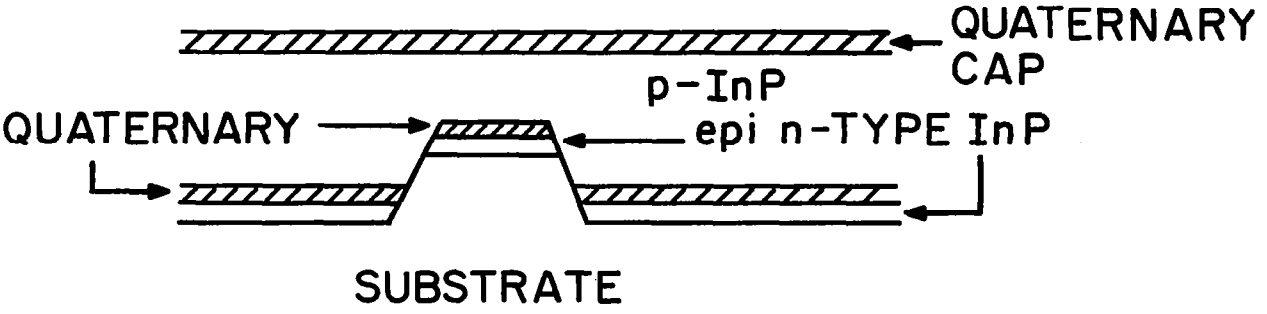

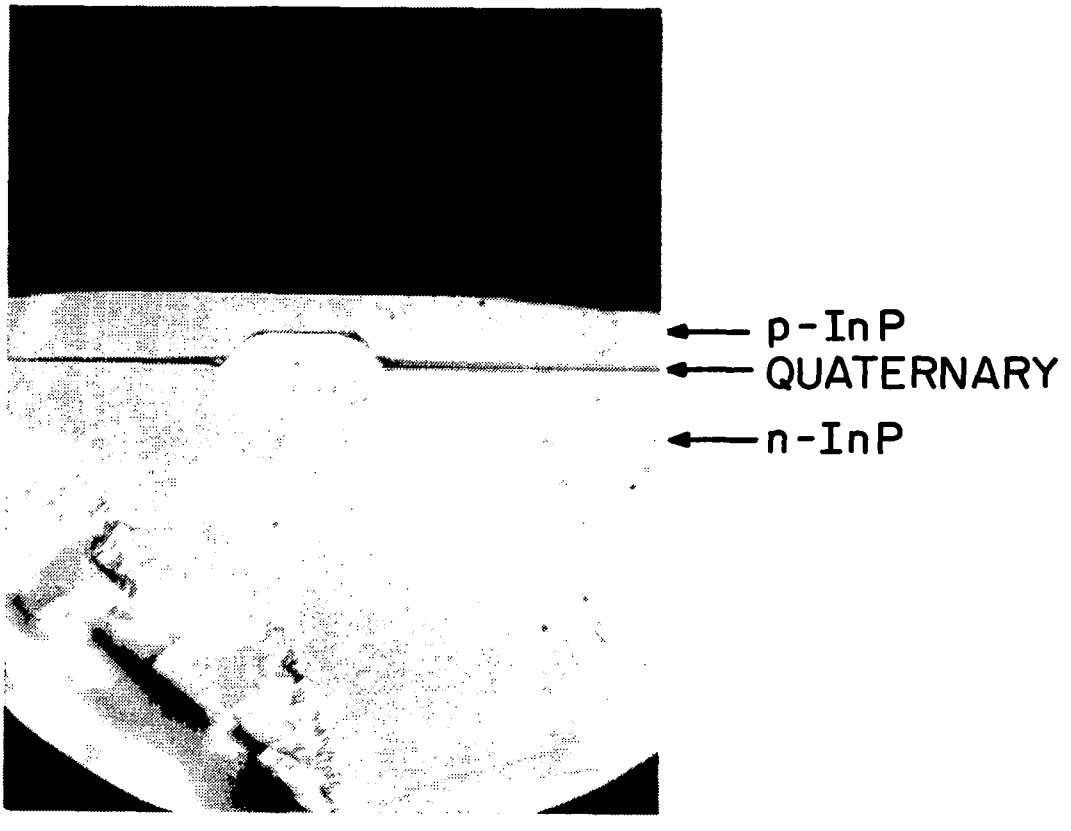

Figure 22. Growth on raised inverted V mesa. The top part of the figure shows the schematic drawing of the grown layers, and the bottom part of the figure shows an etched cross section through a grown structure.

B. DEVICE RESULTS: CDH AND MSBH

1. CDH Type Laser Fabrication

As shown in Fig. 21 a suitably shaped active layer can be obtained by growth over a V-shaped raised mesa. However, as mentioned before, the growth must be properly adapted in order to obtain the correct structure and current flow. Work in this area is still in progress.

2. MSBH Laser Fabrication

After etching raised mesas in the inverted V shape as discussed above, a number of growths were carried out in which all the customary layers were grown sequentially. This included the first InP cladding layer doped with Sn, the InGaAsP quaternary layer, the second p-type cladding layer, and the final InGaAsP cap layer. As shown in Fig. 23(c) the active layer ends up well surrounded by InP. The first InP layer is grown very thin so that no significant side filling occurs, and the same is true of the quaternary active layer. The longer growth period used for the n-type cladding layer causes rapid growth on the mesa sides until an almost planar surface is obtained. The last quaternary layer again serves to facilitate making ohmic contacts. As shown in Figs. 22 and 23, satisfactory structures were obtained. The main difficulty is that the current confinement mechanism does not always work in this structure. In particular, if current is to be channeled to the active layer on top of the mesa without external guiding, a careful adjustment of resistivities in the material will be needed so that the resistance in alternate paths is kept higher than in the direct path to the mesa. In our devices we have so far not optimized the layer resistance. As a consequence, when these devices are excited, one generally observes emission both from the top of the mesa where it is wanted, and from the active layer on the side of the mesa where it is not wanted. The emission in our devices was, therefore, complicated and not single mode. We conclude that

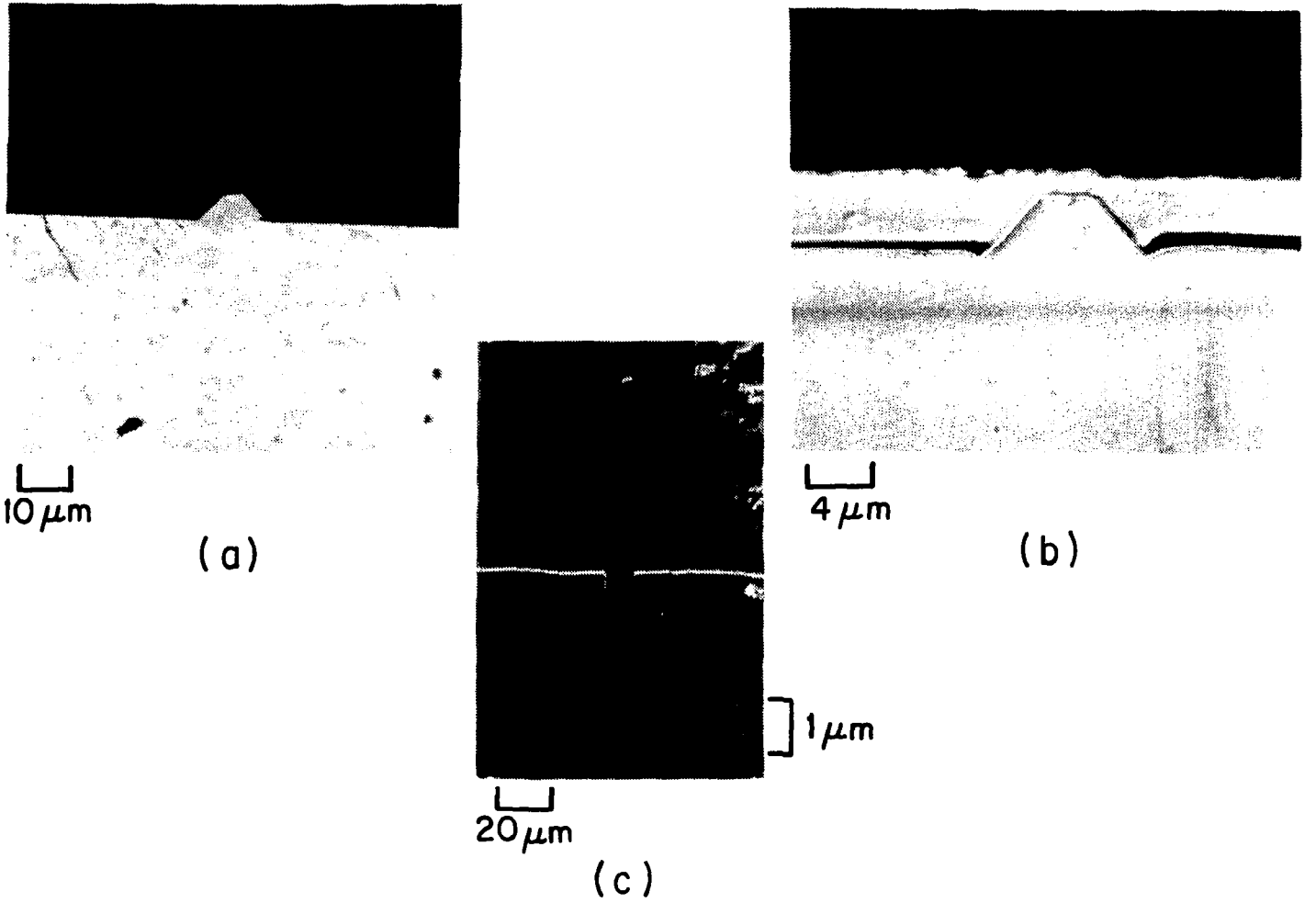

Figure 23. Optical photomicrographs through MSBH type structures grown on inverted V mesas. (a) Shows the substrate after etching, (b) the completed growth, and (c) an angle lap through the grown structure.

more work will be required to control the current path in a satisfactory way.

C. DEVICE RESULTS: BURIED HETEROJUNCTION (BH)

This structure is grown on a raised V type mesa as above, but it does not require critical multiple layer growth since the mesa is etched in previously grown material. Different starting mesas are shown in Fig. 24, all of which allow successful structures to be obtained. Figures 24(a) and (b) show mesas etched in bromine-methanol solutions and Fig. 24(c) shows a mesa etched in iodic acid. A completed structure after regrowth is shown in Fig. 25 using optical photomicrography. The particularly sharp and well-defined active layer surrounded by InP is shown in the SEM photograph in Fig. 26. The near field of such a structure obtained by using an infrared vidicon is displayed in Fig. 27. Figure 27(a) shows an intensity scan through the emitting region (lower trace) and the line where the scan was made (upper trace). The power output in this case was 3 mW and it can be seen that there is a single spot in the near field. At higher powers (~5 mW), Fig. 27(b), the near field breaks up into a higher order mode. In agreement with these results, the spectrum shows several lines at 2 mW and a good single-mode spectrum at 3 mW. This behavior is characteristic of single-mode lasers in contrast with many gain-guided structures which are capable of producing a single-line spectrum right at threshold, but then break up into several lines as the drive is increased. The P-I curve for this device is given in Fig. 29, showing a threshold current of 60 mA.

These results indicate a satisfactory performance level for a single-mode laser and show that the goals of the present contract have been achieved. Further refinement and characterization of this device form the subject of current efforts at RCA Laboratories.

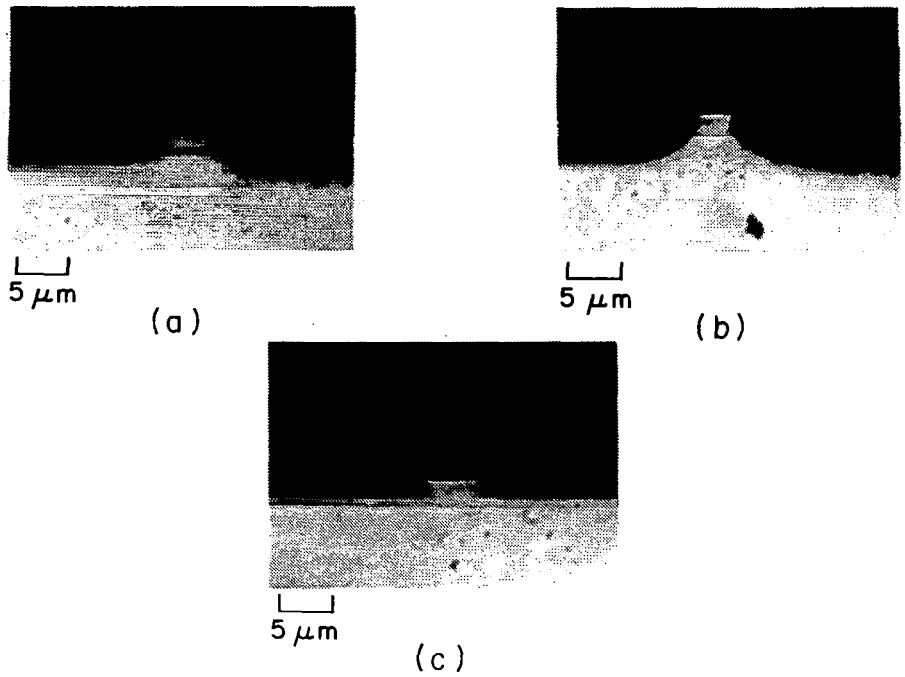

Figure 24. Different mesas etched into grown layers for BH fabrication. (a) and (b) using bromine-methanol, and (c) iodic acid etch.

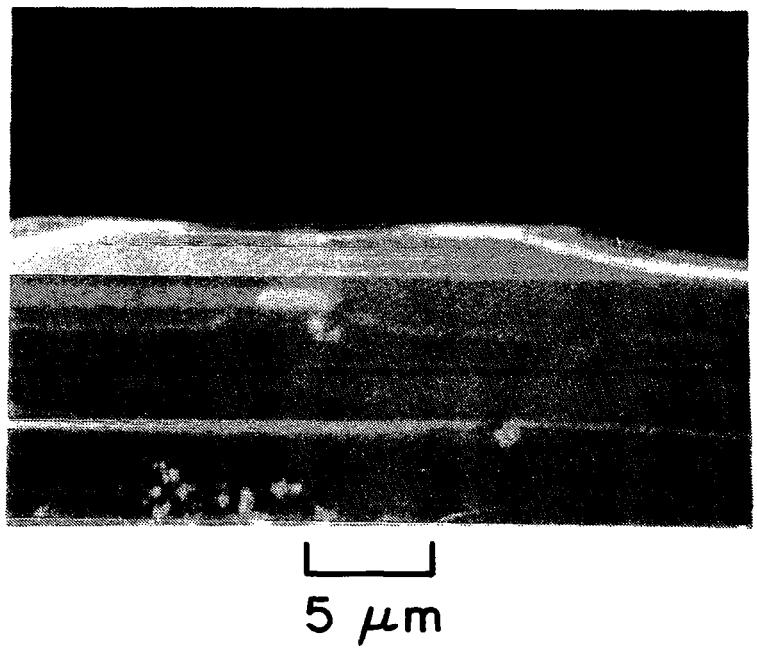

Figure 25. Optical photomicrograph through a BH laser. The well-isolated cavity is clearly visible.

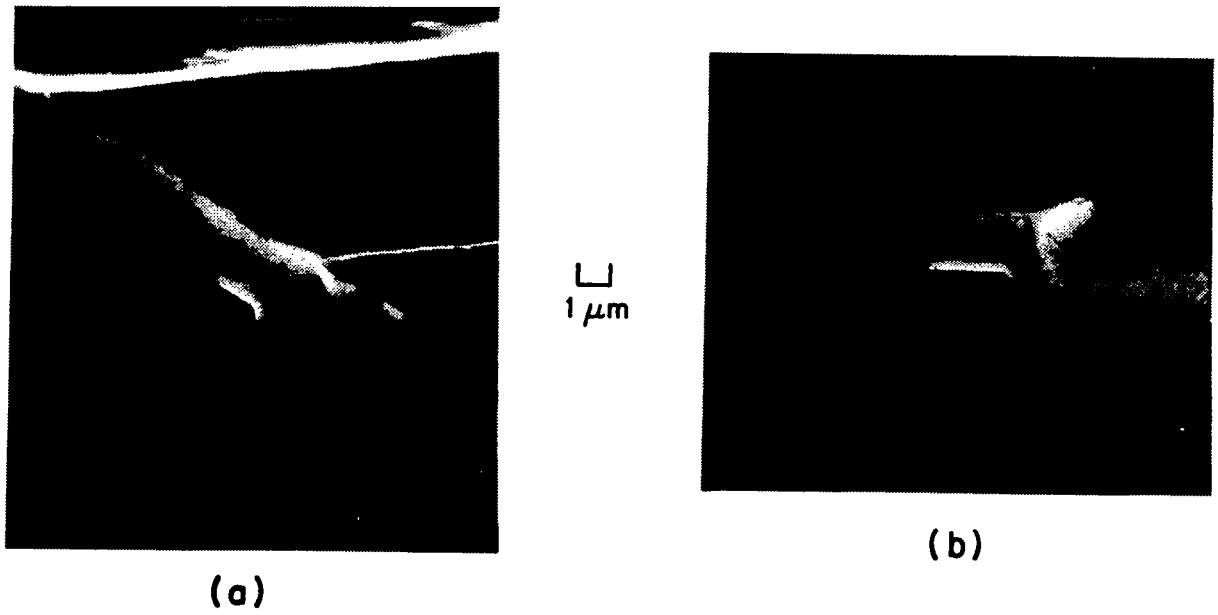

Figure 26. BH cavity as shown by SEM.

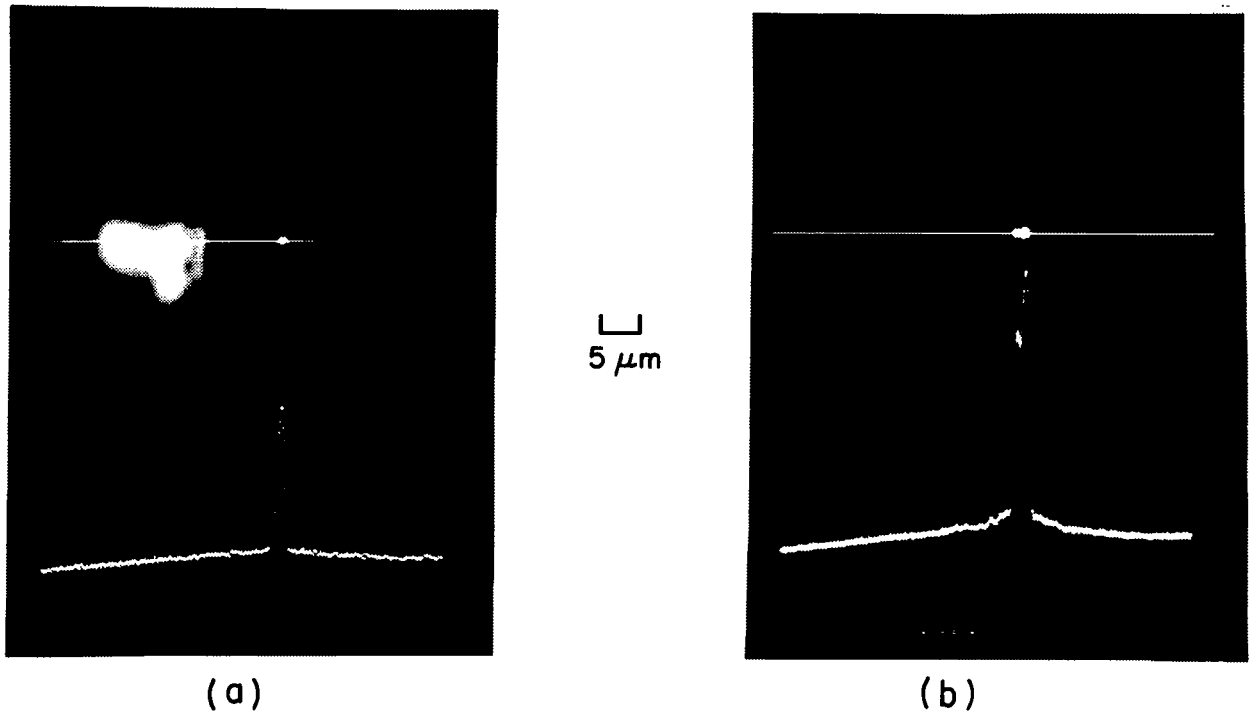

Figure 27. Near field scan through a lasing BH diode, (a) at 3 mW showing a single spot and (b) at 5 mW where the output breaks up into two modes.

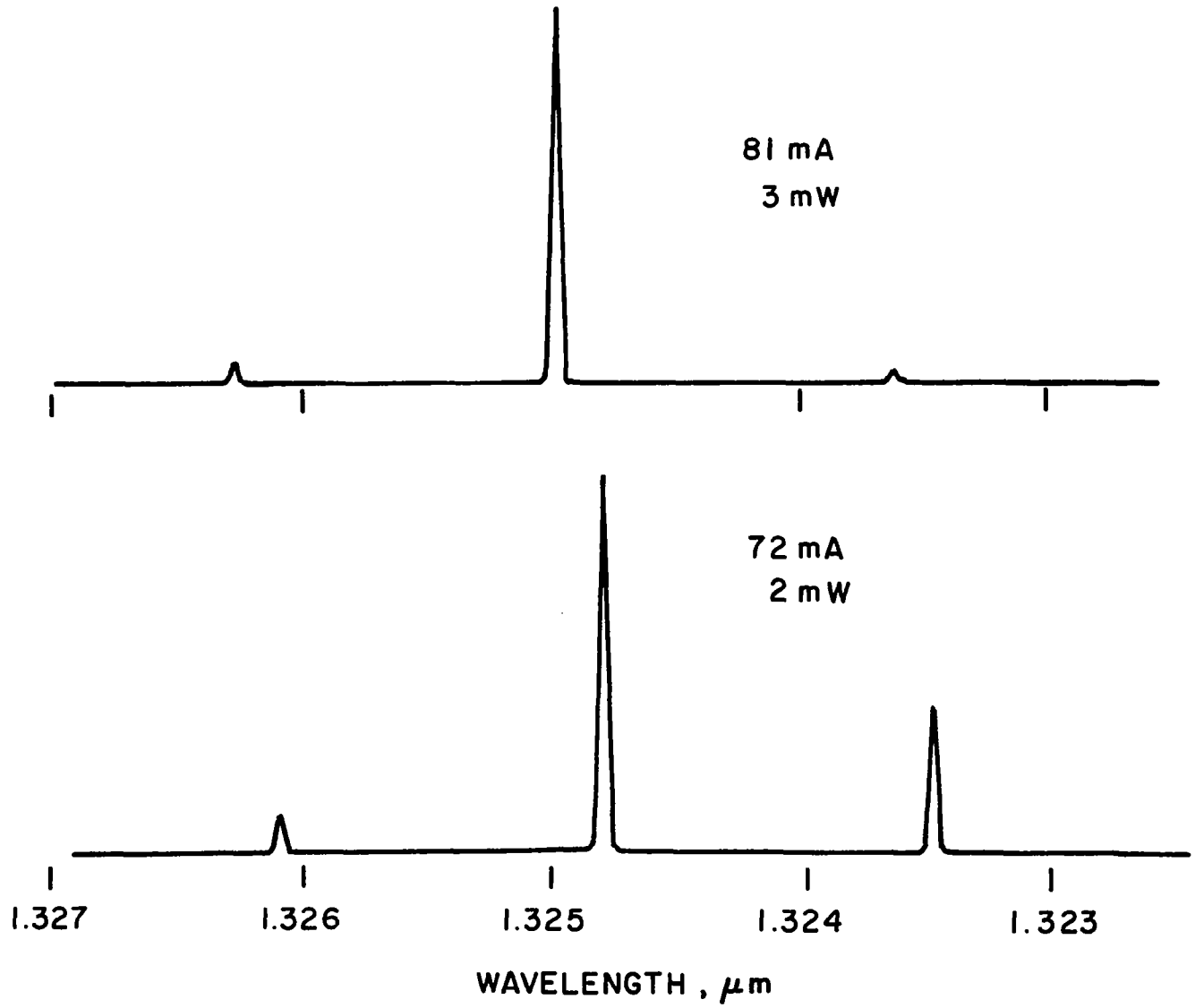

Figure 28. Spectrum of diode of Fig. 27, at two different currents.

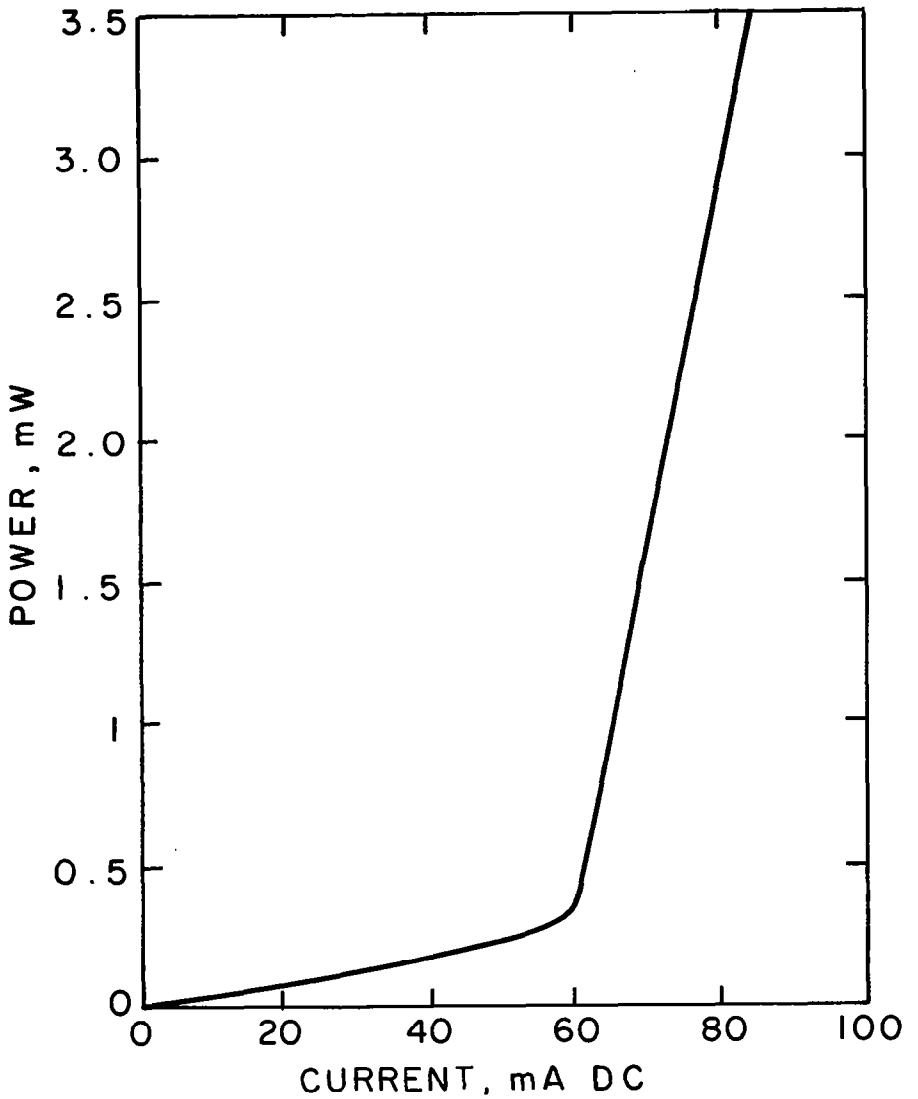

Figure 29. Power-current relation for the laser of Fig. 27.

IV. LONG-WAVELENGTH PHOTODETECTORS

Because of the obvious need for detectors in any NASA contemplated long- wavelength system, a number of RCA-fabricated photodetectors were supplied to NASA Langley for evaluation. These devices were InGaAsP/InP PIN types which respond out to 1.3 μm and InGaAs/InP PIN types which respond to 1.7 μm. They exhibited low leakage current ($\leq$50 nA), high breakdown voltage ($\sim$70 V), and high quantum efficiency (80%) at 1.3 μm. All were of the etched mesa type and have 100-μm-diameter active areas which are ideal for coupling to 50-μm-diameter core silica fibers.

V. CONCLUSIONS

During the course of this program, materials studies as well as general and specific device development were carried out in the InGaAsP system. A comparison was made of three standard methods of evaluating substrate quality by means of dislocation studies. A cause of reduced yield of good wafers, the pullover of melt from one bin to the next, has been analyzed. It has been shown that the pullover of about 70 mg of solution is sufficient to produce visible changes in the X-ray spectrum and to lead to serious increases in the threshold current density. Difficulties with reproducible zinc acceptor doping have been traced to segregation of zinc in the In/Zn alloy used for the doping source. Using EBIC measurements, the pn junction was shown to drift in location depending on factors not always under control. An analysis of contact structures by SIMS showed that the depth to which the sintered Au/Zn contact penetrates into the structure is typically 0.13 μm, or well within the cap layer and out of the p-type cladding and thus should not be deleterious to laser performance. The minimum threshold current density achieved during this contract was 1000 A/cm^2, a significant reduction from the 1500-A/cm^2 value obtained previously.

The problem of single-mode laser development was approached in a systematic manner, and it was shown to be related to the growth habit over four different possible substrate configurations. Raised mesas were found to be more suitable for fabrication than similarly shaped grooves. It was concluded that structures such as BH and MSBH are especially desirable in that they conform to the natural growth habit of the LPE grown InGaAsP material on (100) oriented wafers.

A new geometry has been proposed, which is similarly advantageous, and which lends itself to the fabrication of CDH type structures. The fabrication of CDH, MSBH, and BH structures was discussed, and

measurements were presented on the device properties of single-mode buried heterostructure lasers made in the course of this contract. Results include single spectral line emission at 3 mW and a threshold current of 60 mA.

REFERENCES

1. I. Ladany, F. Z. Hawrylo, R. T. Smith, and E. R. Levin: Study of LPE Methods for Growth of InGaAsP/InP CW Lasers. NASA CR-3268, 1980.
2. A. Huber and N. T. Linh: Revelation Metallographique des Defauts Cristallins dans InP. J. Cryst. Growth, vol. 29, 1975, pp. 80-84.
3. M. B. Small and R. Ghez: Growth and Disolution Kinetics of III-V Heterostructures Formed by LPE. J. Appl. Phys., vol. 50, 1979, pp. 5322-5330.
4. E. V. K. Rao, M. Quillec, J. L. Benchimol, and H. Thibierge: Photoluminescence Study of Perturbed Growth of InP on Quaternary Layers in InGaAsP-InP Double Heterostructures. Appl. Phys. Lett., vol. 37, 1980, pp. 228-231.
5. M. A. Pollack, R. E. Nahory, J. C. DeWinter, and A. A. Ballman: Liquid Phase Epitaxial $In_{1-x}Ga_xAs_yP_{1-y}$ Lattice-Matched to (100) InP over the Complete Wavelength Range $0.92 \leq \lambda \leq 1.65$ um. Appl. Phys. Lett., vol. 33, 1978, pp. 314-316.
6. J. J. Hsieh: Thickness and Surface Morphology of GaAs LPE Layers Grown by Supercooling, Step-Cooling, Equilibrium-Cooling and Two-Phase Solution Techniques. J. Cryst. Growth, vol. 27, 1974, pp. 49-61.
7. G. H. Olsen, T. Z. Zamerowski, R. T. Smith, and E. P. Bertin. InGaAsP Quarternary Alloys: Composition, Refractive Index, and Lattice Mismatch. J. Electron. Mat., vol. 9, 1980, pp. 977-987.
8. A. Onton, M. R. Lorenz, and W. Reuter: Electronic Structure and Luminescence Processes in $In_{1-x}Ga_xP$ Alloys. J. Appl. Phys., vol. 42, 1971, pp. 3420-3432.
9. I. Ladany and F. Z. Hawrylo: Comparison of Single- and Two-Phase LPE Growth Methods for InGaAsP/InP Lasers and LEDs. J. Cryst. Growth, vol. 54, 1981, pp. 69-75.
10. M. Ettenberg, H. S. Sommers, Jr., H. Kressel, and H. G. Lockwood: Control of Facet Damage in GaAs Laser Diodes. Appl. Phys. Lett., vol. 18, 1971, pp. 571-573.

1. Report No.	2. Government Accession No.	3. Recipient's Catalog No.
NASA CR-3477		

4. Title and Subtitle	5. Report Date
InGaAsP/InP Laser Development for Single-Mode, High-Data-Rate Communications	November 1981
	6. Performing Organization Code
7. Author(s)	8. Performing Organization Report No.
I. Ladany, E.R. Levin, C.W. Magee, R.T. Smith	PRRL-81-CR-12
9. Performing Organization Name and Address	10. Work Unit No.
RCA Laboratories Princeton, NJ 08540	11. Contract or Grant No. NAS1-15962
12. Sponsoring Agency Name and Address	13. Type of Report and Period Covered
National Aeronautics and Space Administration Washington, DC 20546	Contractor Report 7-1-80 to 3-31-81
	14. Sponsoring Agency Code

15. Supplementary Notes

Langley Technical Monitor: Herbert D. Hendricks
Interim Report on Phase I

16. Abstract

During the course of this program, materials studies as well as general and specific device development were carried out in the InGaAsP system. A comparison was made of three standard methods of evaluating substrate quality by means of dislocation studies. A cause of reduced yield of good wafers, the pullover of melt from one bin to the next, has been analyzed. It has been shown that the pullover of about 70 mg of solution is sufficient to produce visible changes in the X-ray spectrum and to lead to serious increases in the threshold current density. Difficulties with reproducible zinc acceptor doping have been traced to segregation of zinc in the In/Zn alloy used for the doping source. Using EBIC measurements, the pn junction was shown to drift in location depending on factors not always under control. An analysis of contact structures by SIMS showed that the depth to which the sintered Au/Zn contact penetrates into the structure is typically 0.13 μm, or well within the cap layer and out of the p-type cladding and thus not deleterious to laser perfprmance. The minimum threshold current density achieved during this contract was 1000 A/cm^2, a significant reduction from the 1500 A/cm^2 value obtained previously.

The problem of single-mode laser development was approached in a systematic manner, and it was shown to be related to the growth habit over four different possible substrate configurations. Raised mesas were found to be more suitable for fabrication than similarly shaped grooves. It was concluded that structures such as BH and MSBH are especially desirable in that they conform to the natural growth habit of the LPE grown InGaAsP material on (100) oriented wafers.

A new geometry has been proposed, which is similarly advantageous, and which lends itself to the fabrication of CDH type structures. The fabrication of CDH, MSBH, and BH structures was discussed, and measurements were presented on the device properties of single-mode buried heterostructure lasers made in the course of this contract. Results include single spectral line emission at 3 mW and a threshold current of 60 mA.

17. Key Words (Selected by Author(s))		18. Distribution Statement
In/Ga/As/P	LASERS	Unclassified - Unlimited
INDEX-GUIDED STRUCTURES	DEVICES	
BURIED HETEROSTRUCTURE		
MATERIALS		Subject Category 36

19. Security Classif. (of this report)	20. Security Classif. (of this page)	21. No. of Pages	22. Price
Unclassified	Unclassified	59	A04

For sale by National Technical Information Service, Springfield, Virginia 22161.

NASA-Langley, 1981